Supplementary Information (SI) for Dalton Transactions.
This journal is © The Royal Society of Chemistry 2024

# Highly selective organo-gallium hydroxamate mediated inhibition of antibiotic resistant *Klebsiella pneumoniae*

Rebekah N Duffin, Jenisi TA Kelderman, Megan E Herdman and Philip C Andrews

School of Chemistry, Monash University, Clayton, Melbourne, VIC, Australia 3800

1. $^{1}$H and $^{13}$C NMR Spectroscopy of gallium complexes
2. FT-IR Spectra of Metal Complexes **1 – 6**
3. High Resolution ESI-MS on Metal Complexes **1 – 6**
4. Additional Analytical Data
5. Biological Testing
6. Experimental Section for Complexes **7, 8, 9** and **10**
7. X-ray Crystallography
8. Biological Images

# 1. $^{1}H$ and $^{13}C$ NMR Spectroscopy of Gallium Complexes

$^{1}H$ NMR [Ga(BPHA)$_3$] **1** in d$_6$ – DMSO

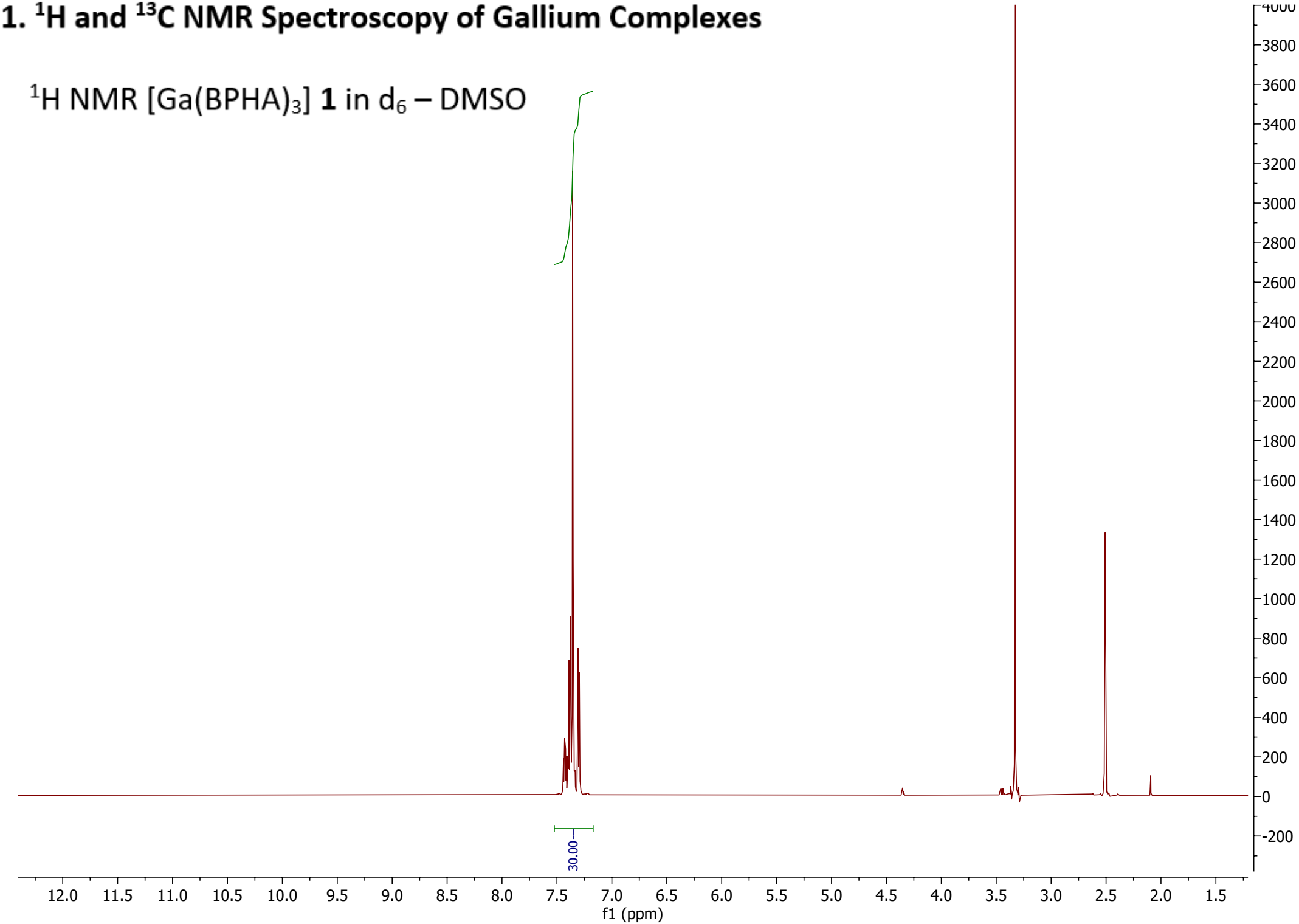

$^{13}C$ NMR [Ga(BPHA)$_3$] **1** in d$_6$ – DMSO

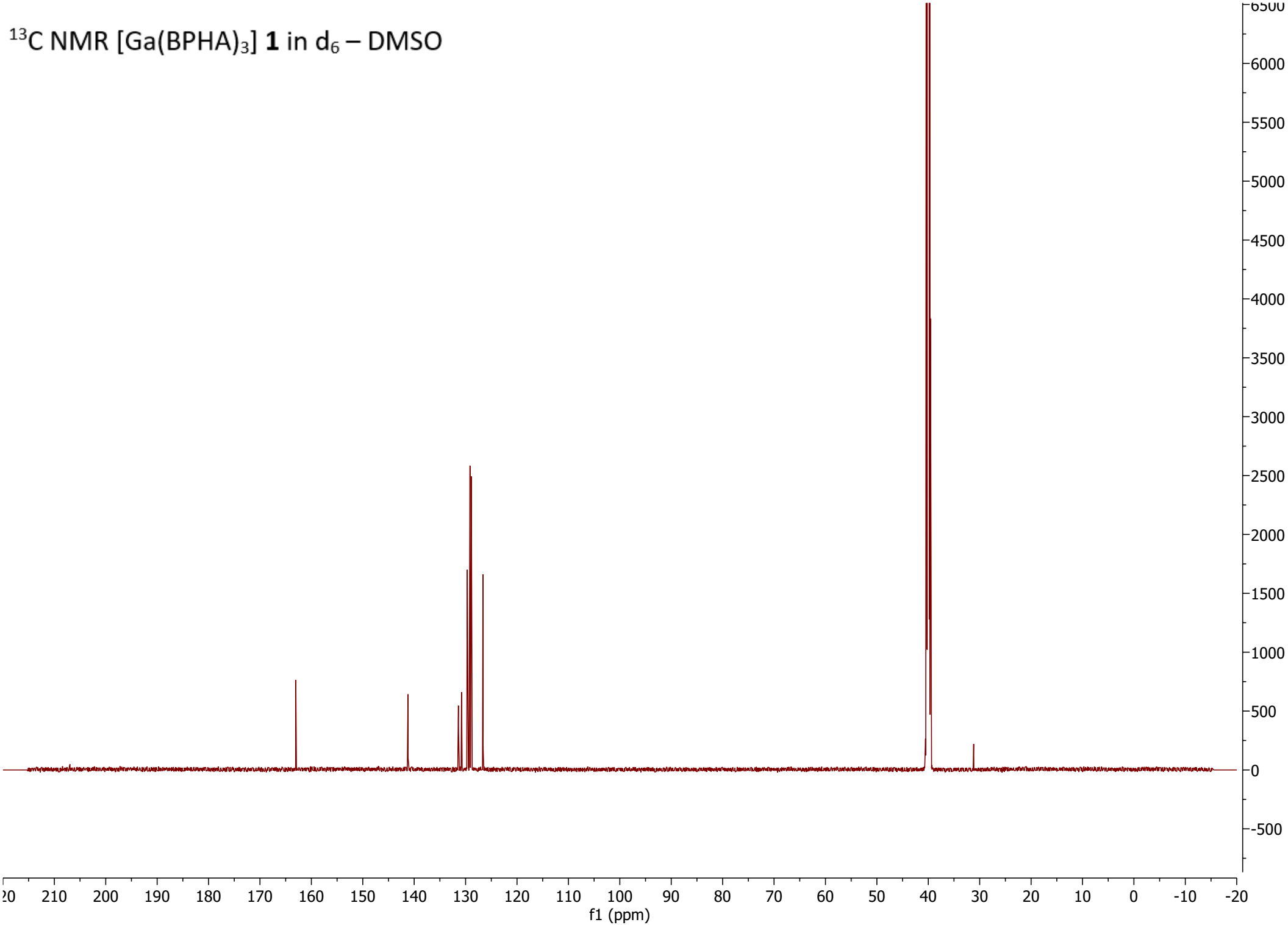

$^{1}$H NMR [Ga(BHA-*H*)$_3$] **2** in d$_6$ – DMSO

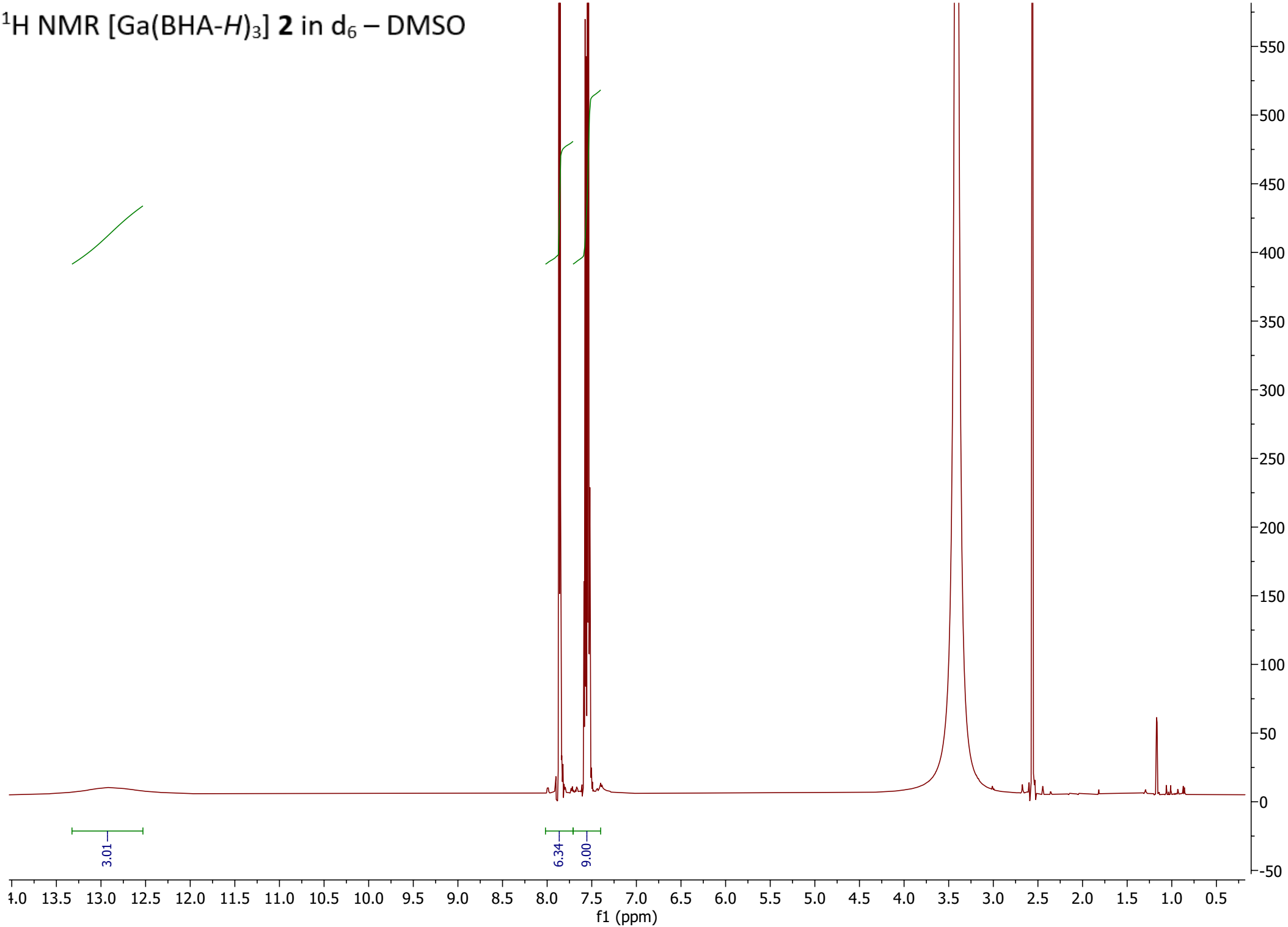

$^{13}$C NMR [Ga(BHA-*H*)$_3$] **2** in d$_6$ – DMSO

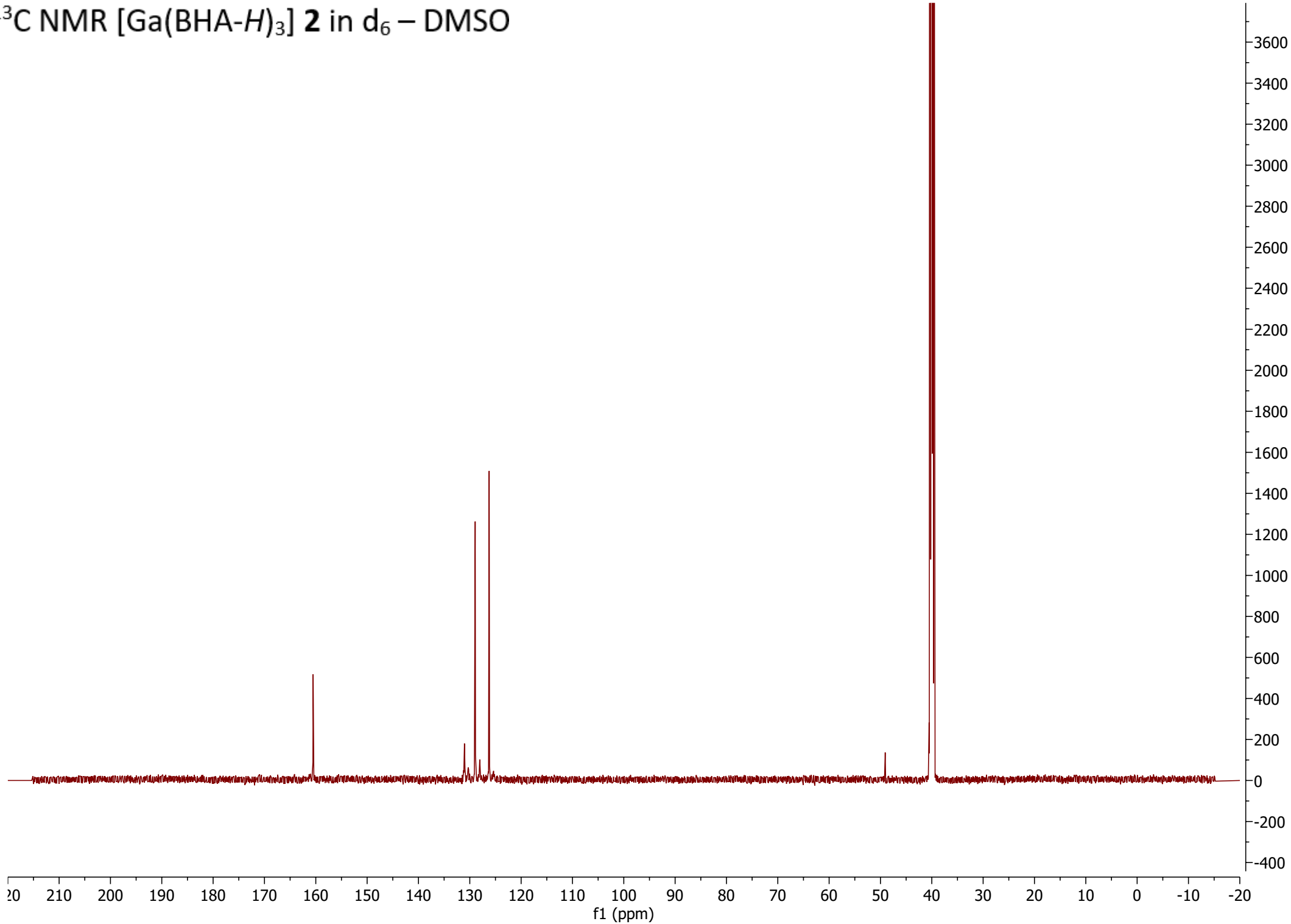

$^{1}$H NMR [Ga(SHA-$H_2$)(SHA-$H$)] **3** and [Ga(SHA-$H$)$_3$] in d$_6$ – DMSO

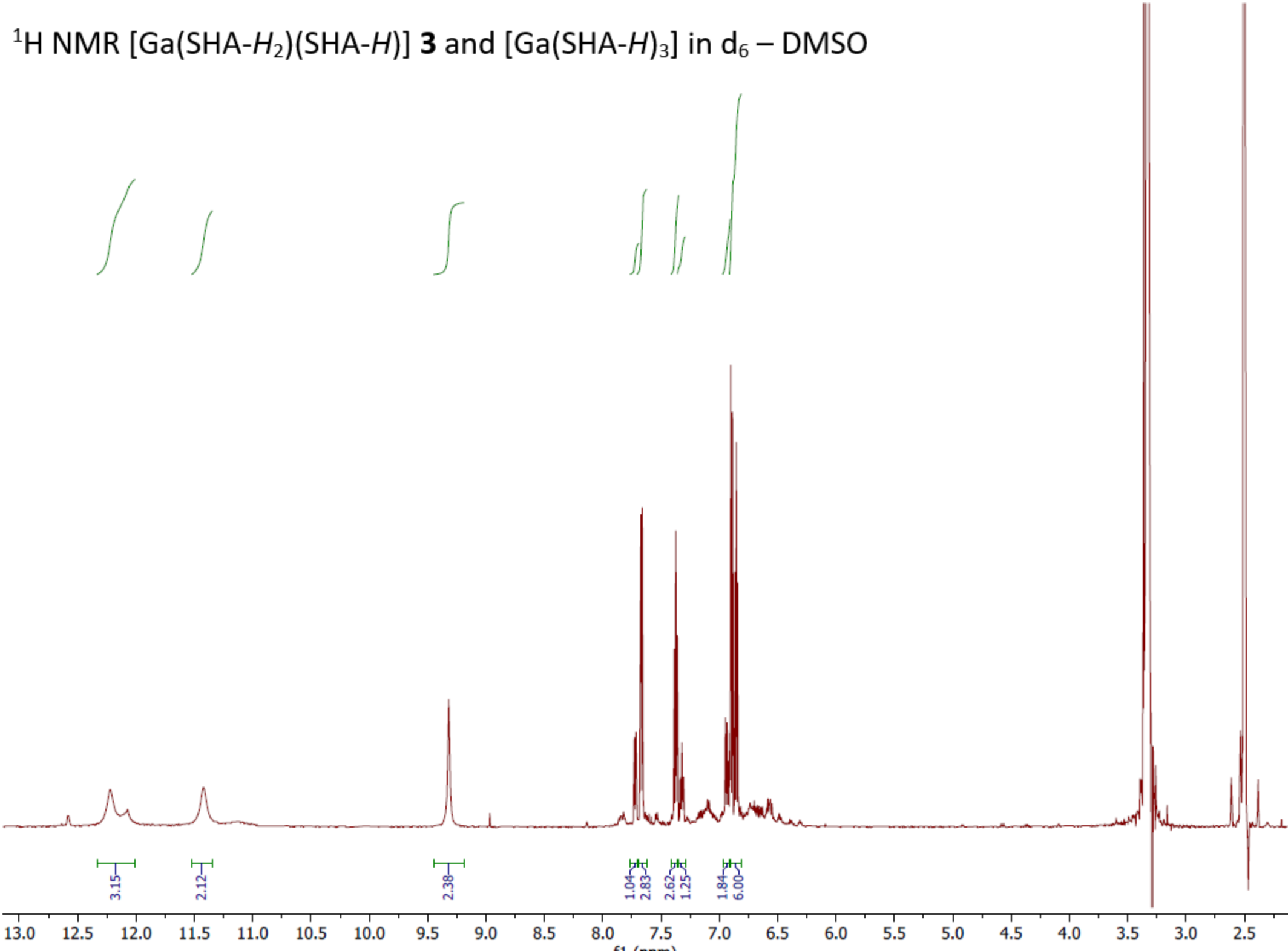

$^{13}$C NMR [Ga(SHA-*H*$_2$)(SHA-*H*)] **3** and [Ga(SHA-*H*)$_3$] in d$_6$ – DMSO

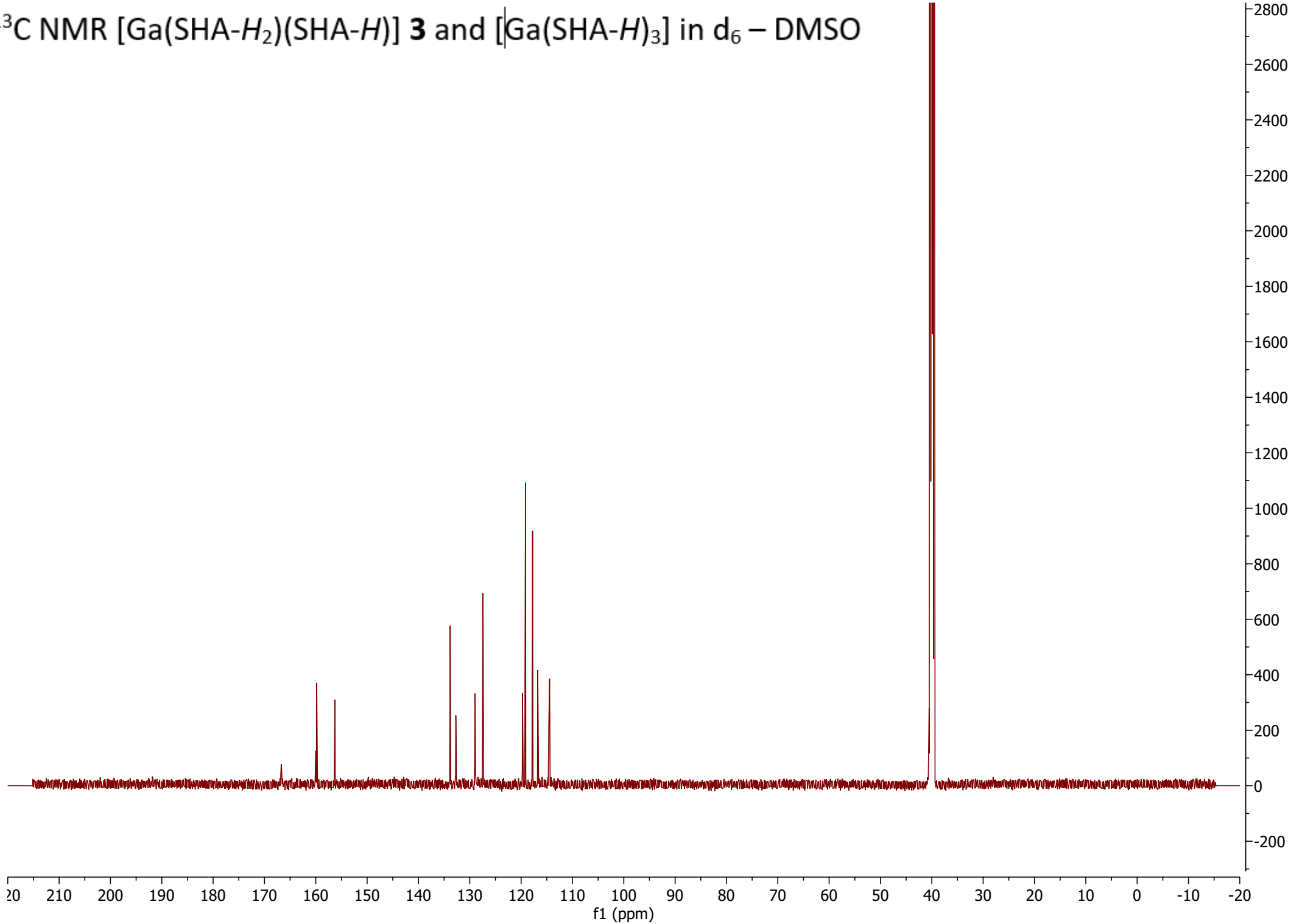

$^{1}$H NMR [$GaMe_2$(BPHA)] **4** in $d_6$ – DMSO

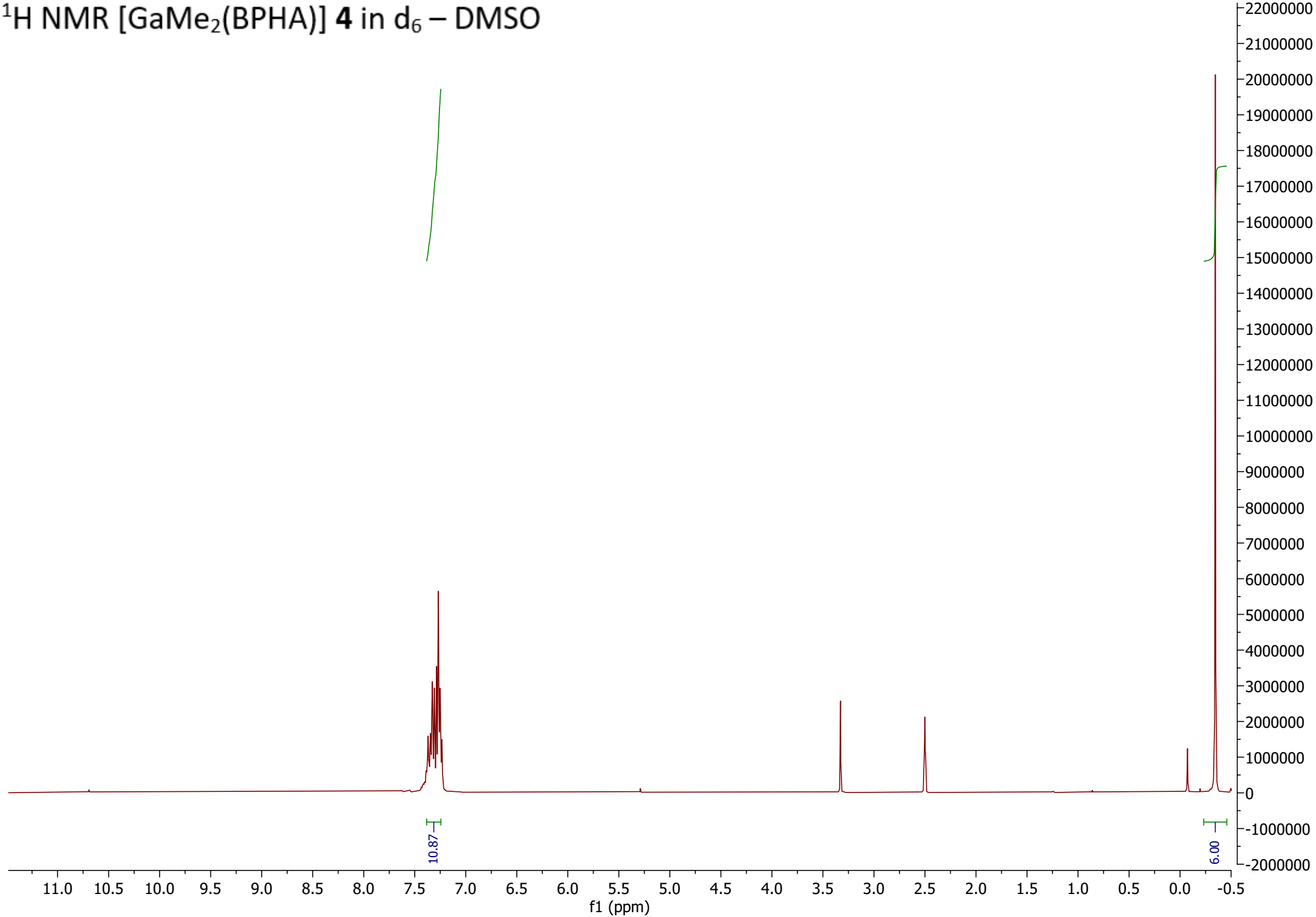

$^{13}C$ NMR [$GaMe_2$(BPHA)] **4** in $d_6$ – DMSO

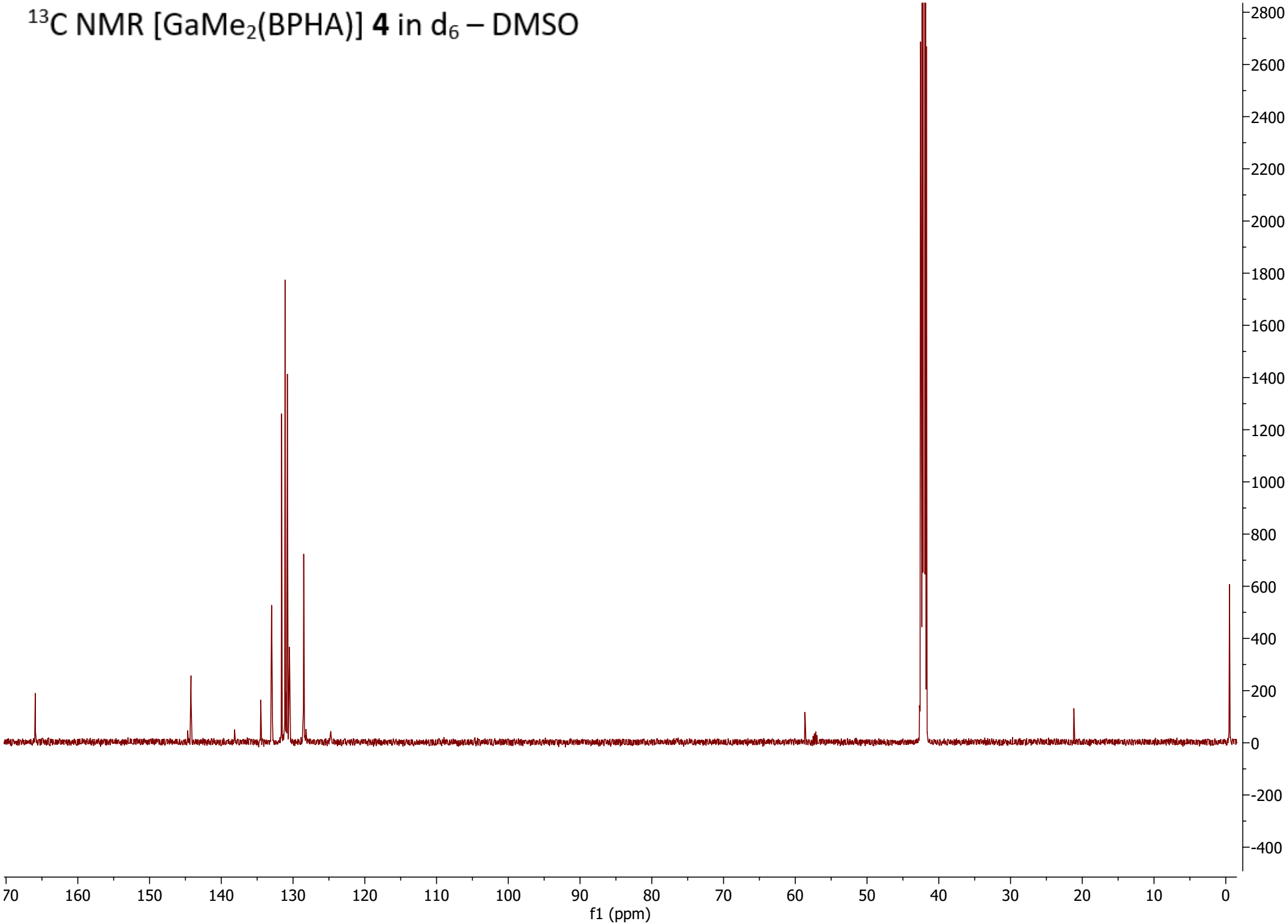

$^{1}$H NMR [GaMe(BHA-*H*)$_2$] **5** in d$_6$ – DMSO

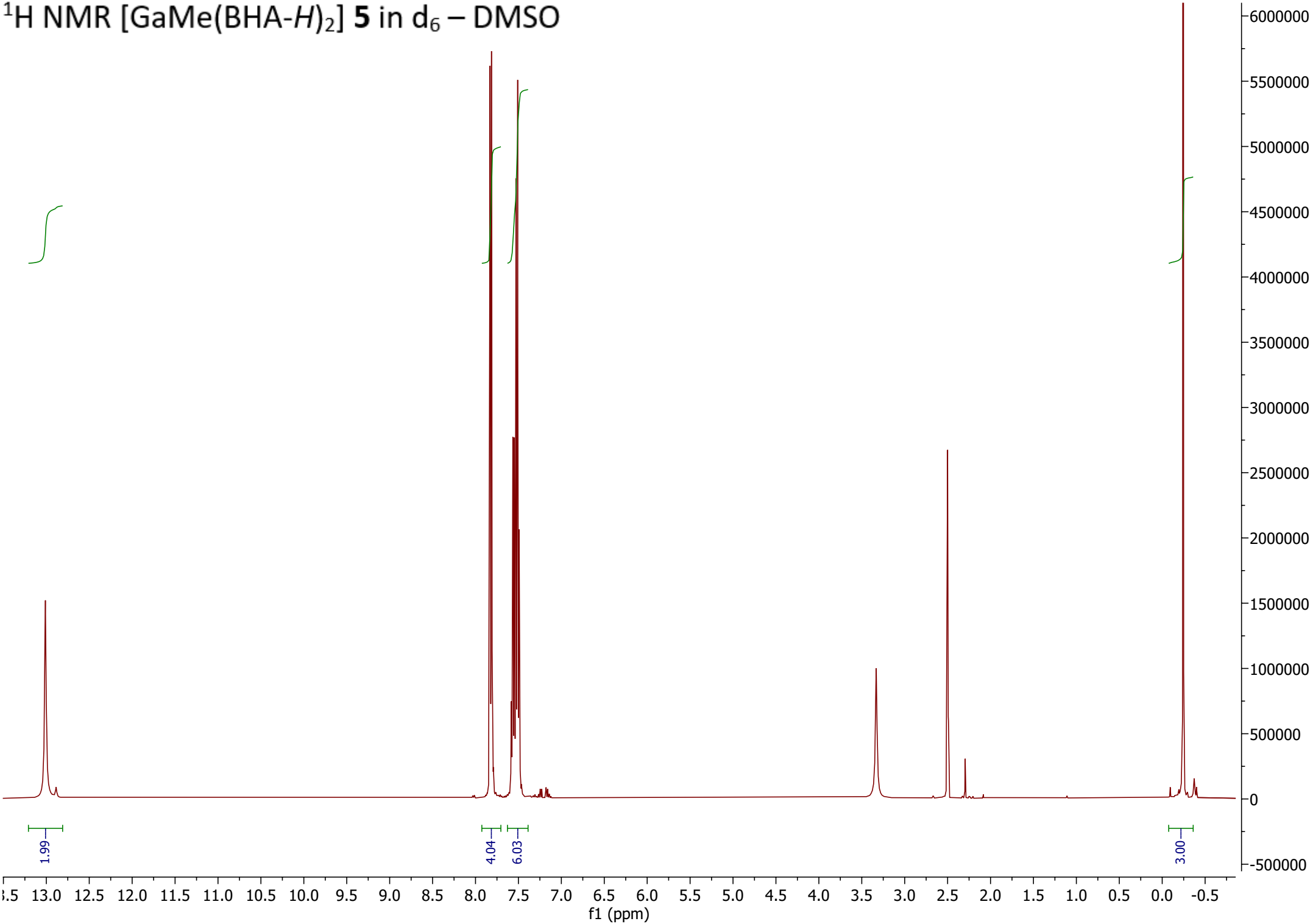

$^{13}$C NMR [GaMe(BHA-*H*)$_2$] **5** in d$_6$ – DMSO

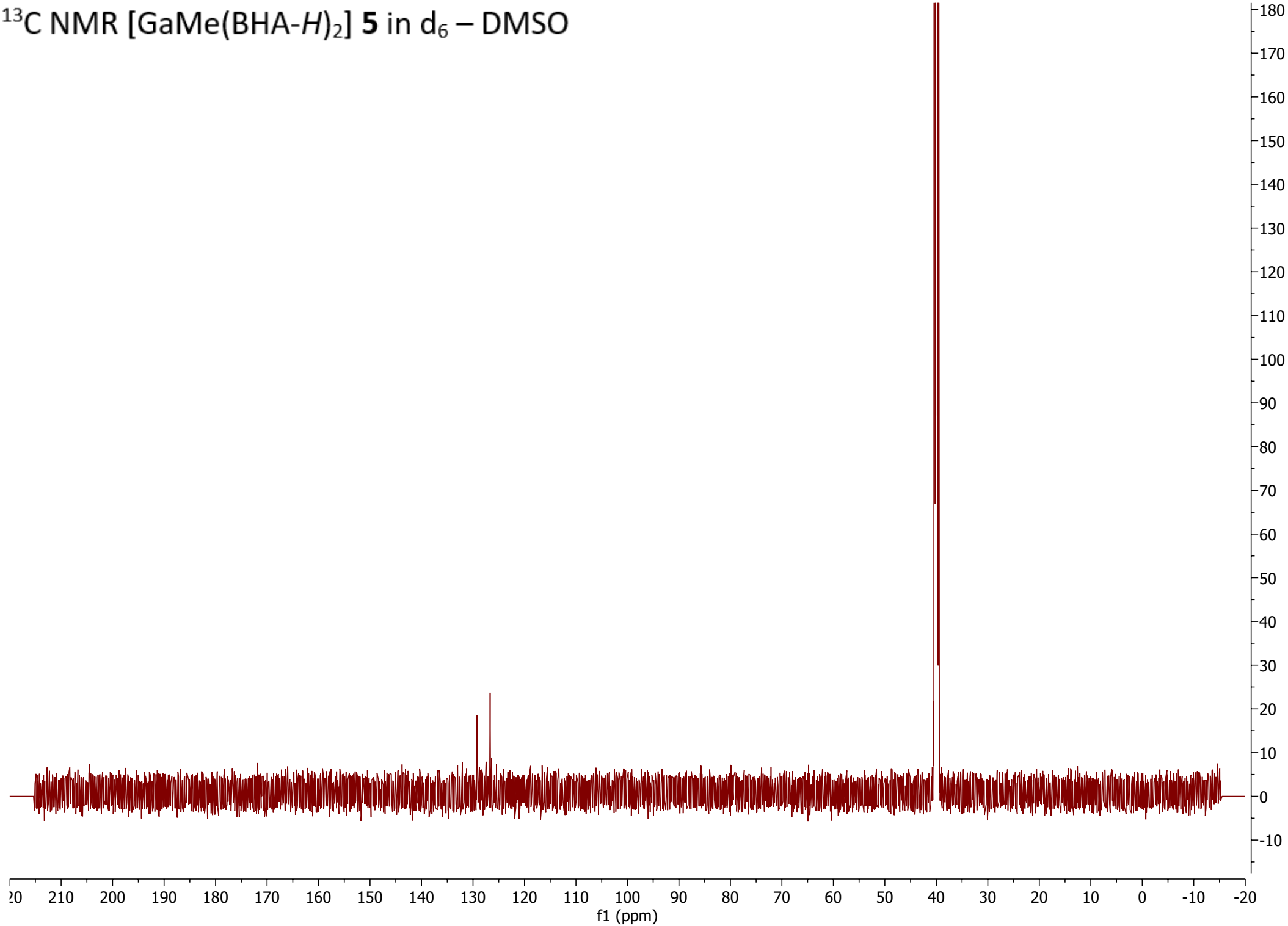

H NMR of [GaMe2(OH)] in DMSO-d6

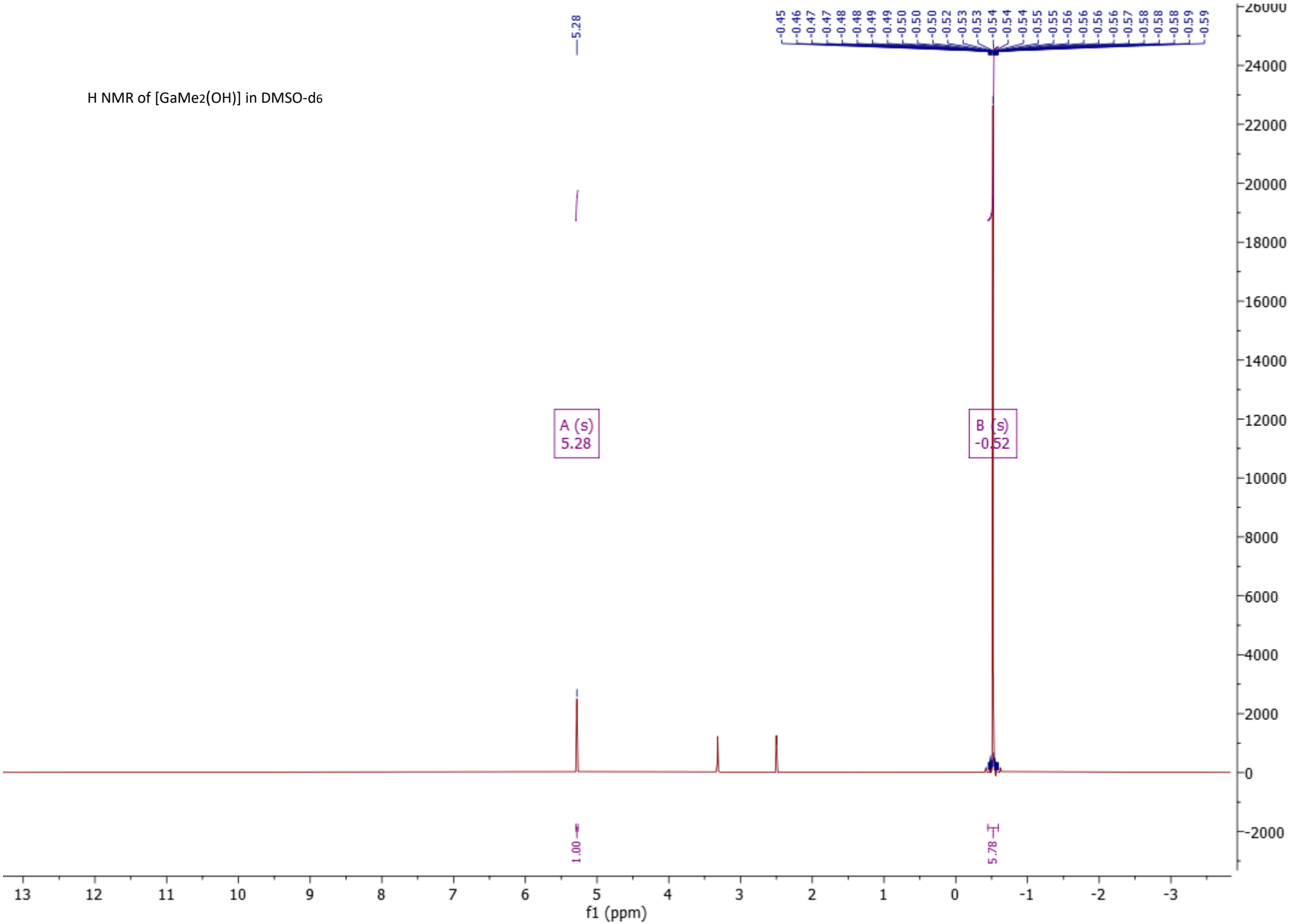

Stacked 1H NMR of free BPHAH, complex 1 and complex 4, highlighting shifts in the signals and the absence of the acid proton

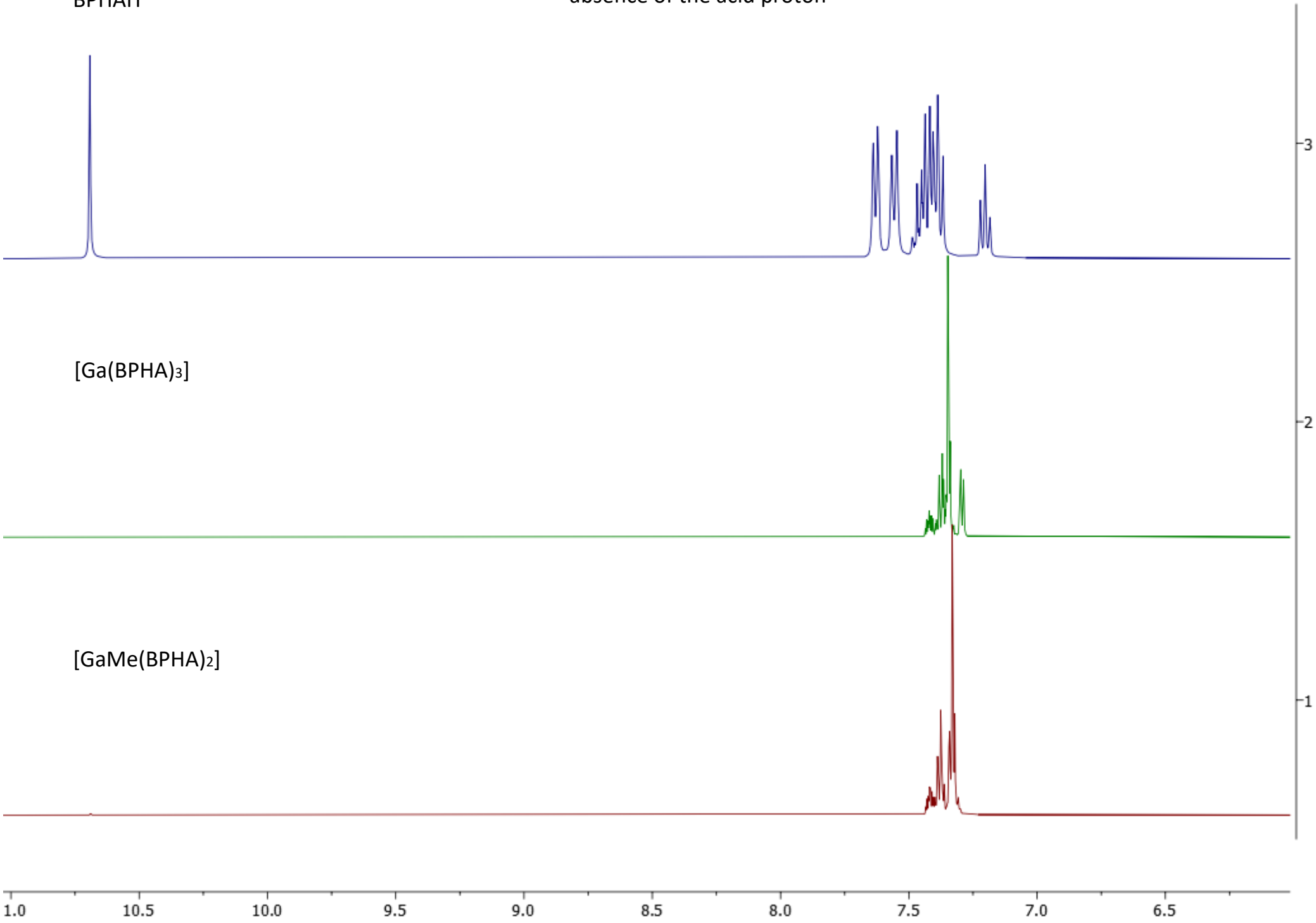

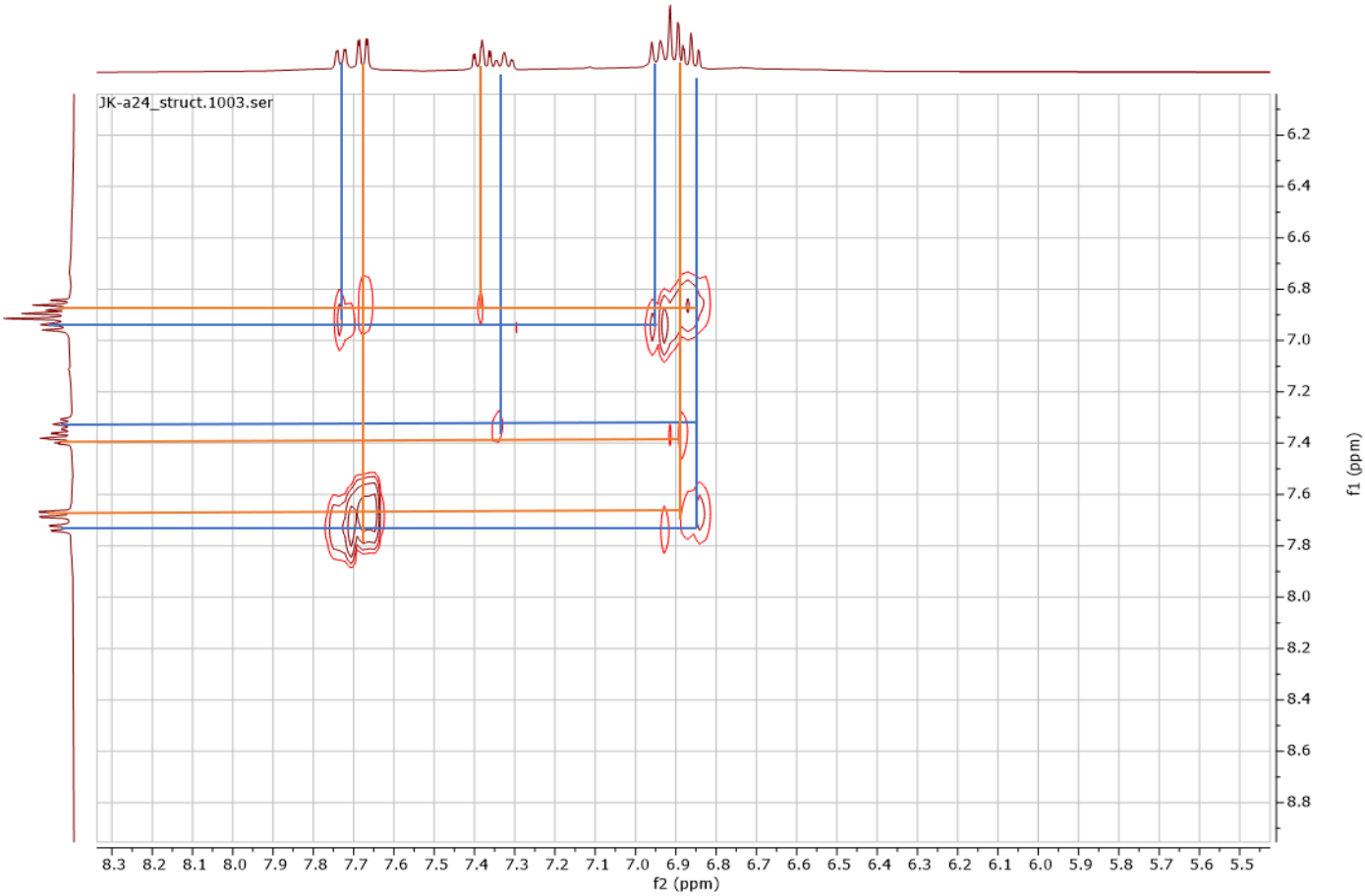


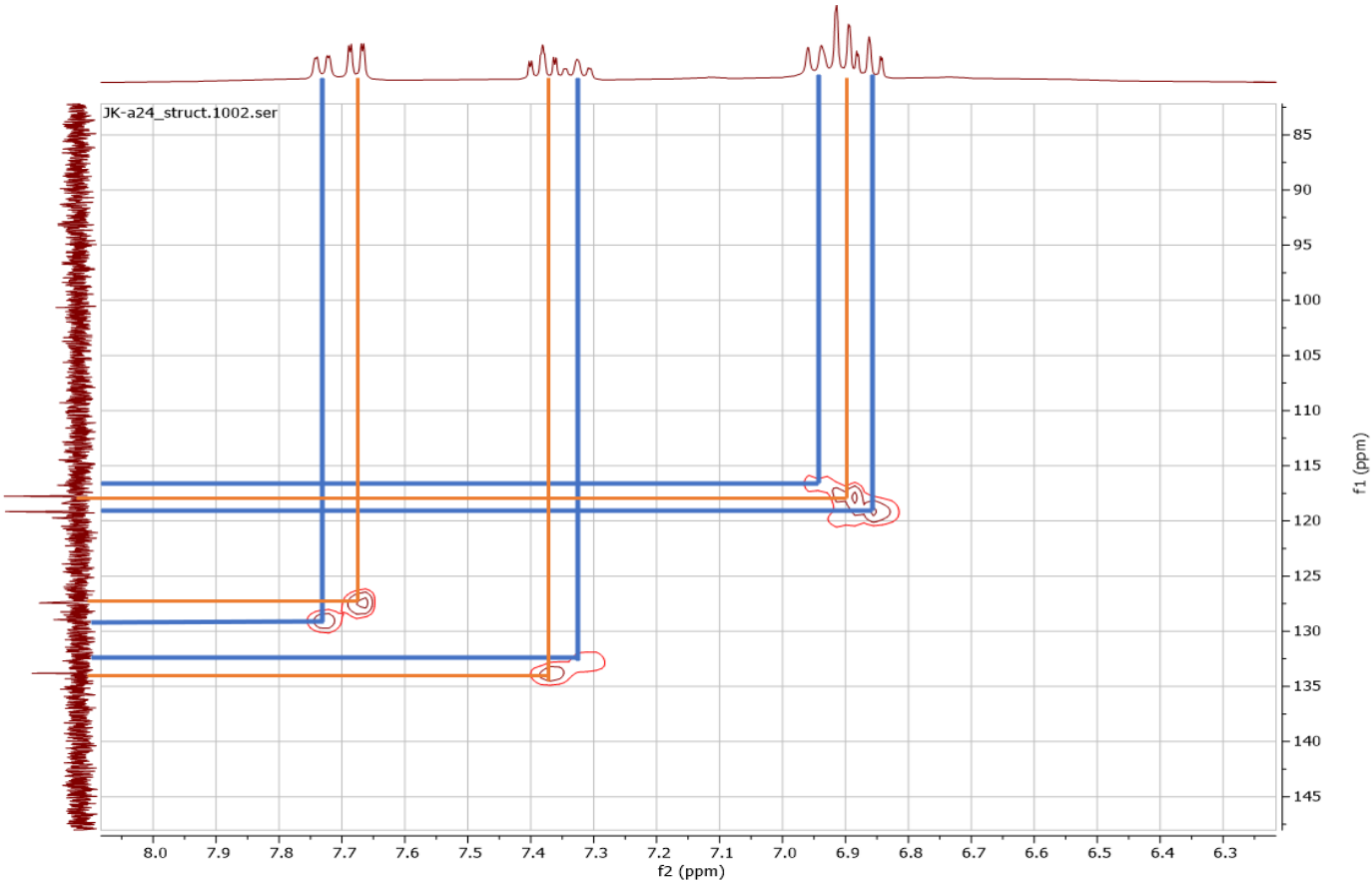


2-D proton-proton and proton-carbon correlation spectra for complex 3 in the solution state.

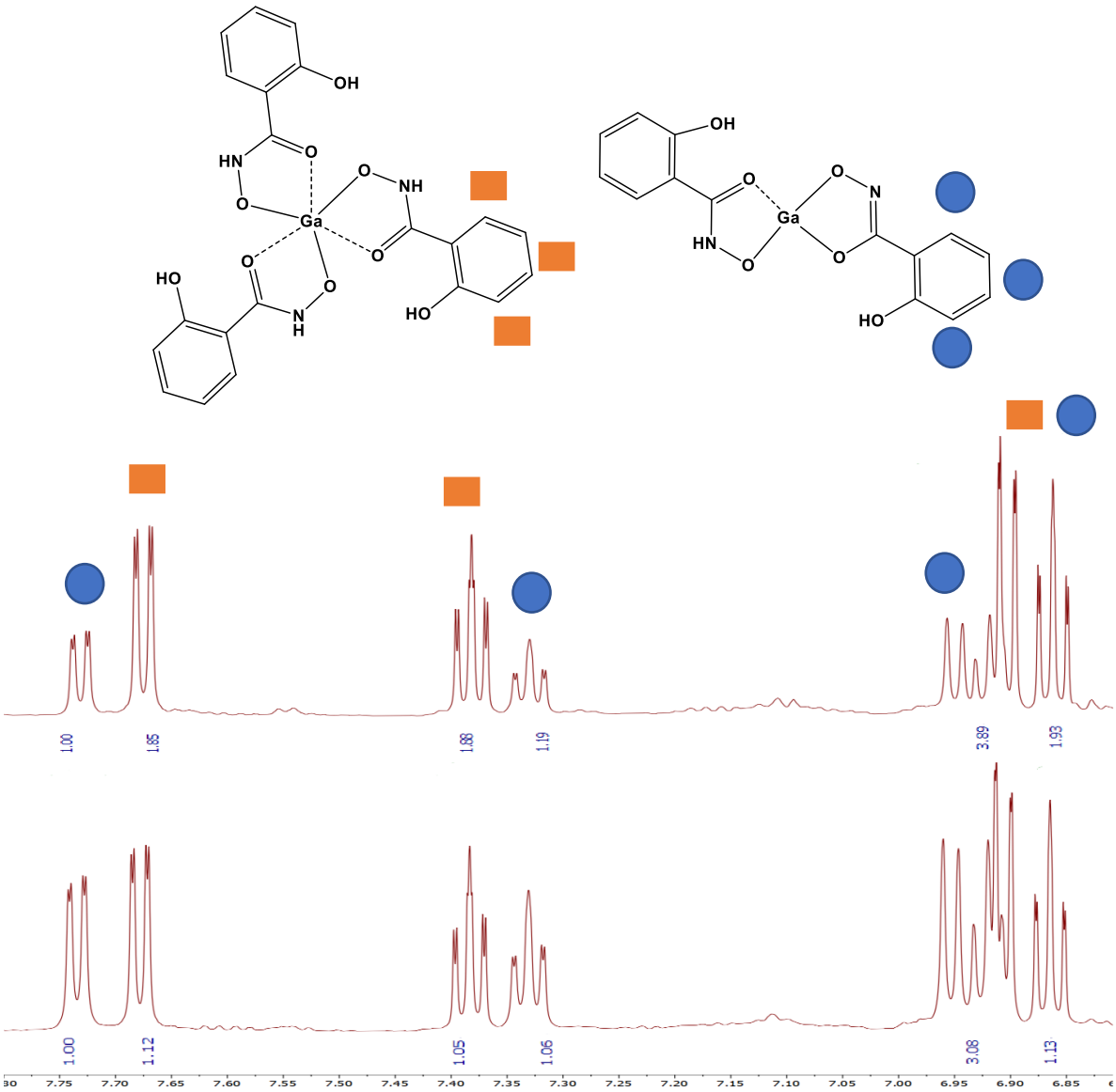


Figure S1. $^{1}$H NMR stack of two individual spectra of complex **3,** highlighting the changes in the aromatic region in regards to the changes in the enol-keto ratio.

## 2. FT-IR Spectra of Metal Complexes 1 - 6

**1**, $[Ga(BPHA)_3]$

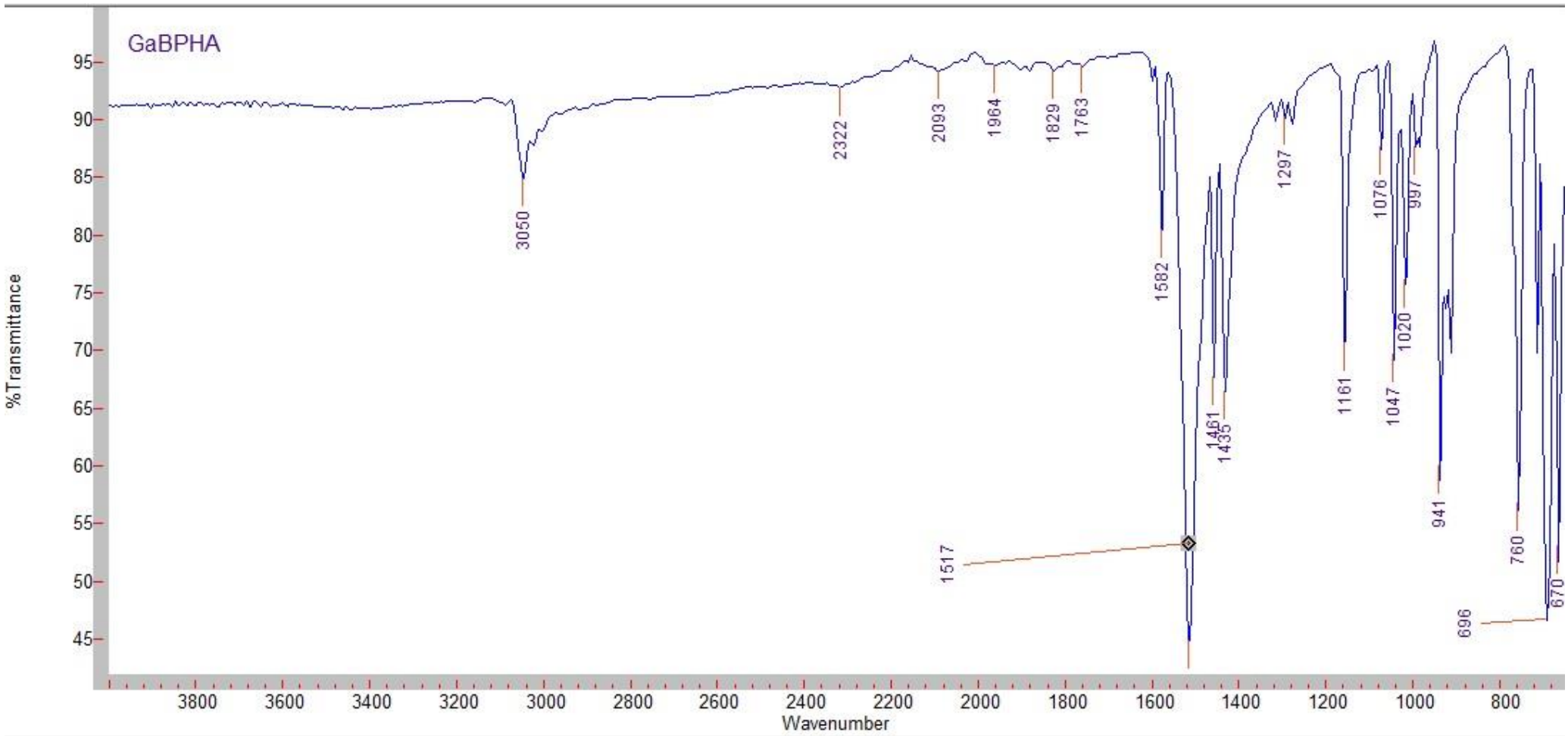

**2**, $[Ga(BHA)_3]$

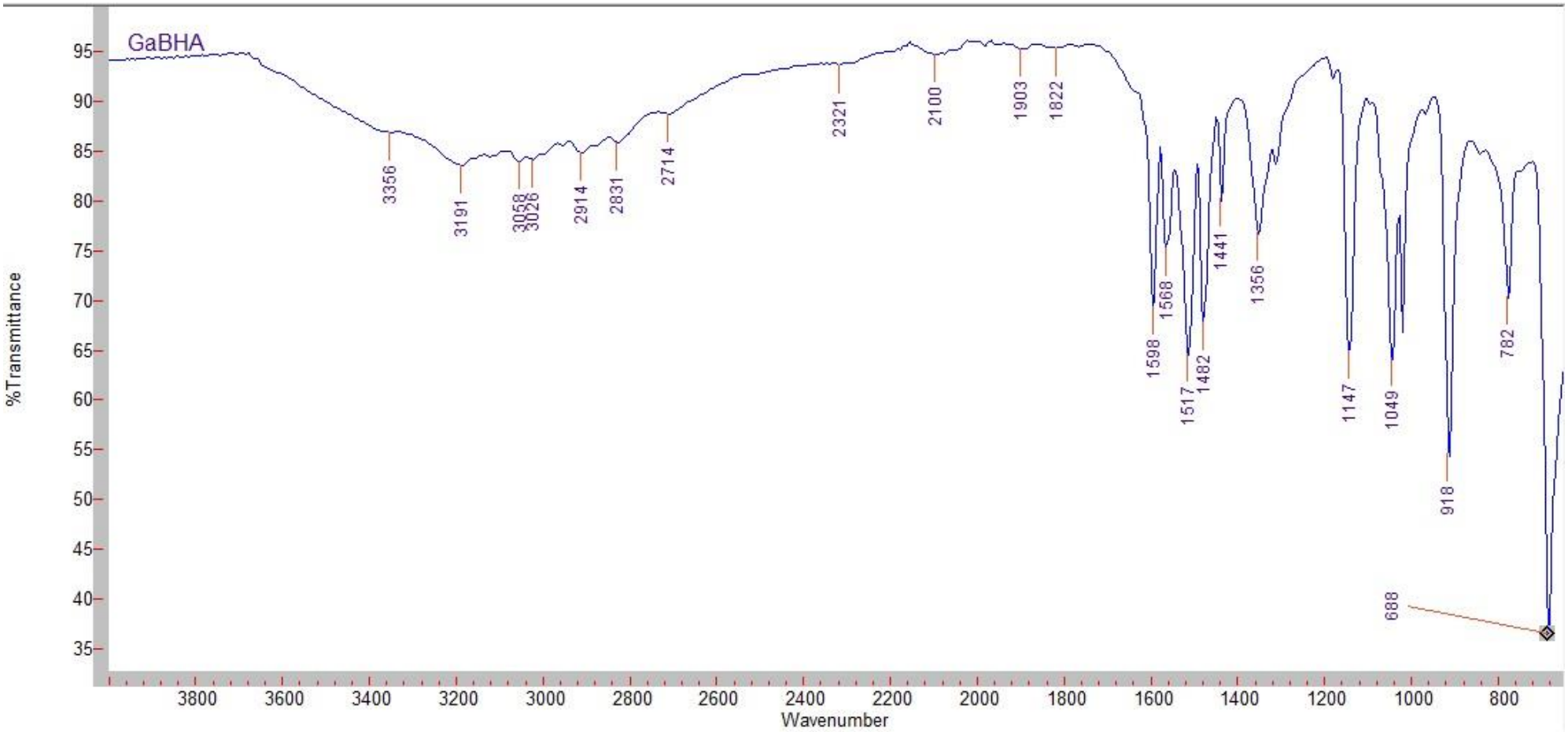
GaBHA
%Transmittance
Wavenumber
3356
3191
3058
3026
2914
2831
2714
2321
2100
1903
1822
1598
1568
1517
1482
1441
1356
1147
1049
918
782
688

**3**, [Ga(SHA-$H_2$)(SHA-$H$)]

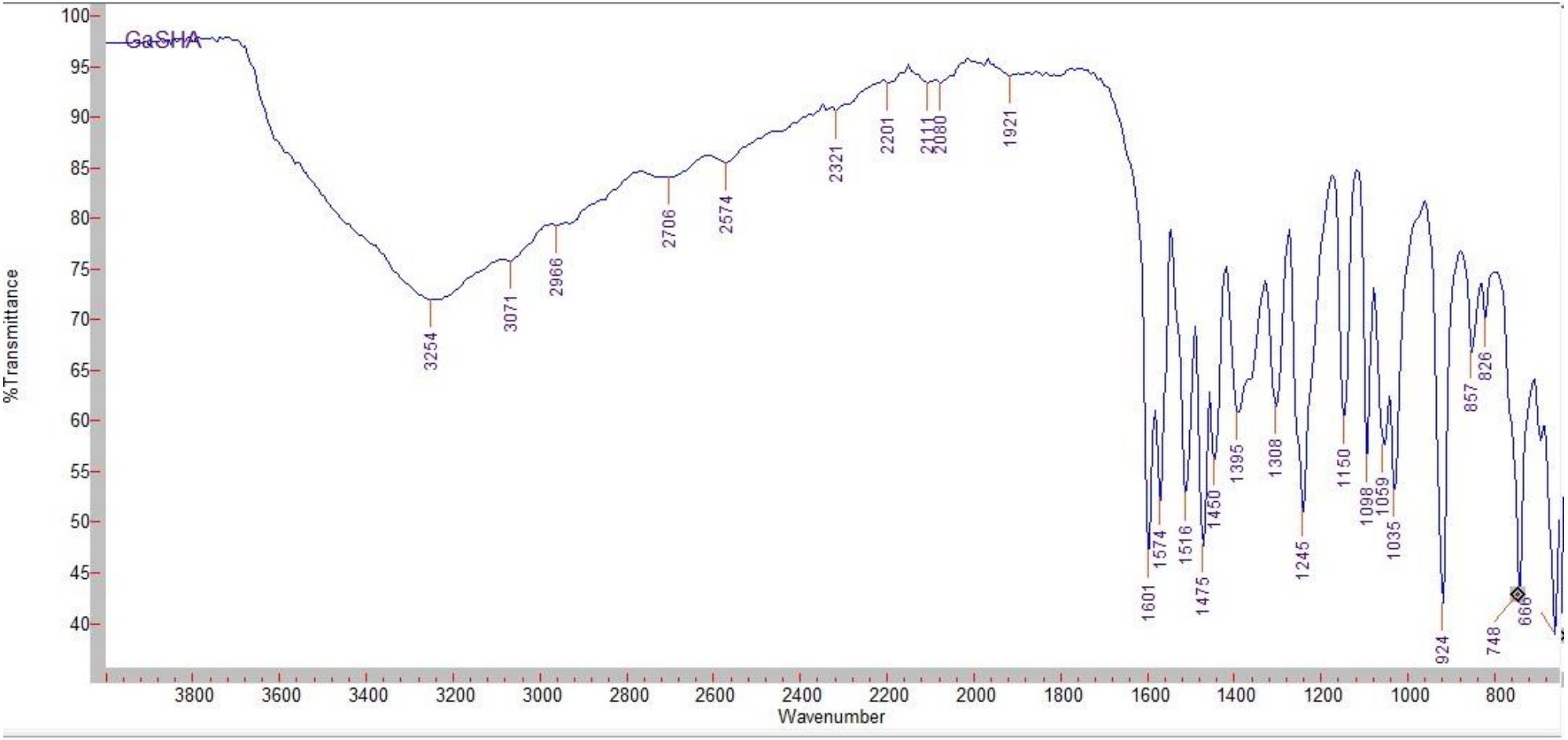

**4,** [$GaMe_2$(BPHA)]

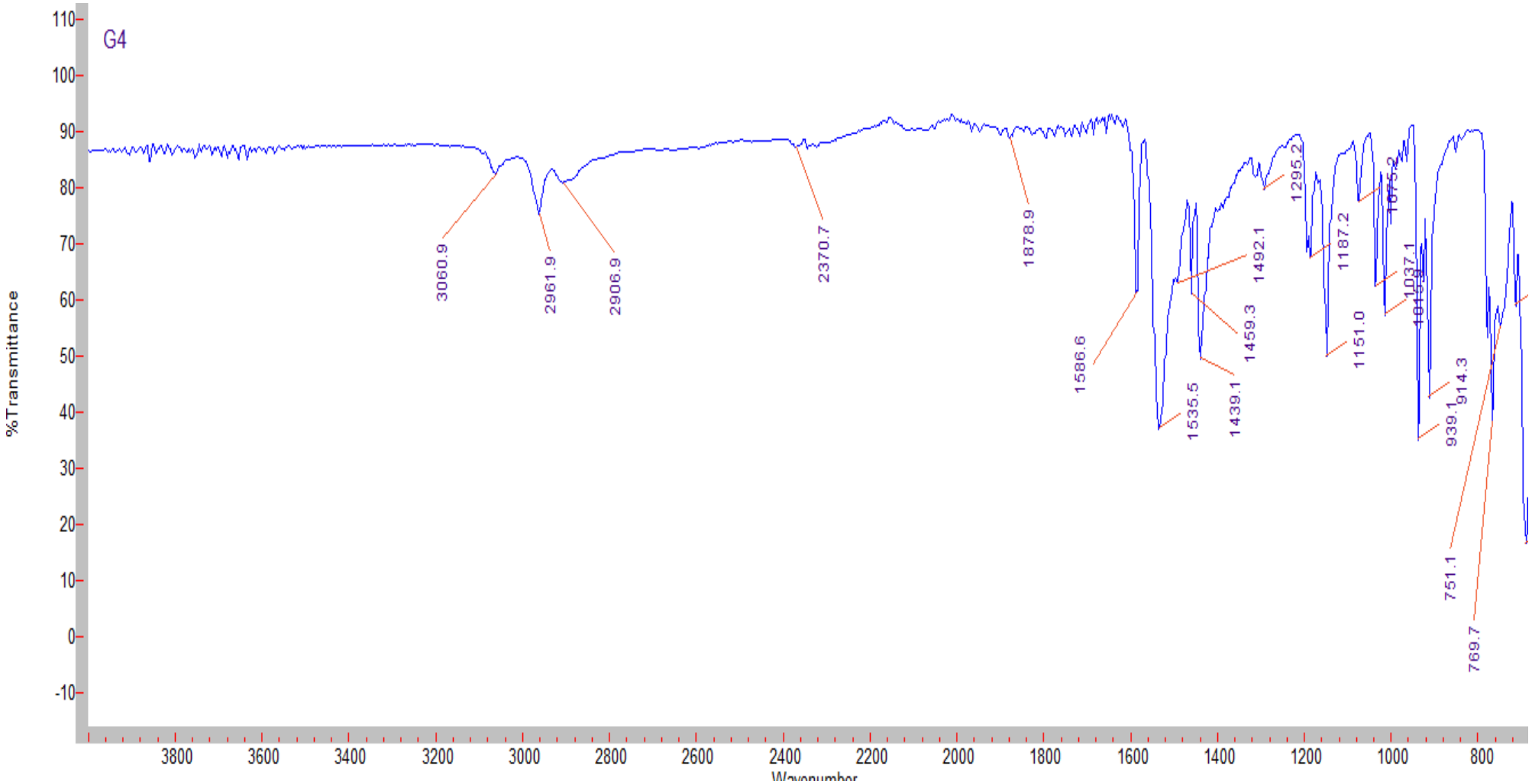
G4
%Transmittance
Wavenumber
3060.9
2961.9
2906.9
2370.7
1878.9
1586.6
1535.5
1439.1
1459.3
1492.1
1295.2
1187.2
1151.0
1037.1
939.1
914.3
751.1
769.7

**5**, [GaMe(BHA)$_2$]

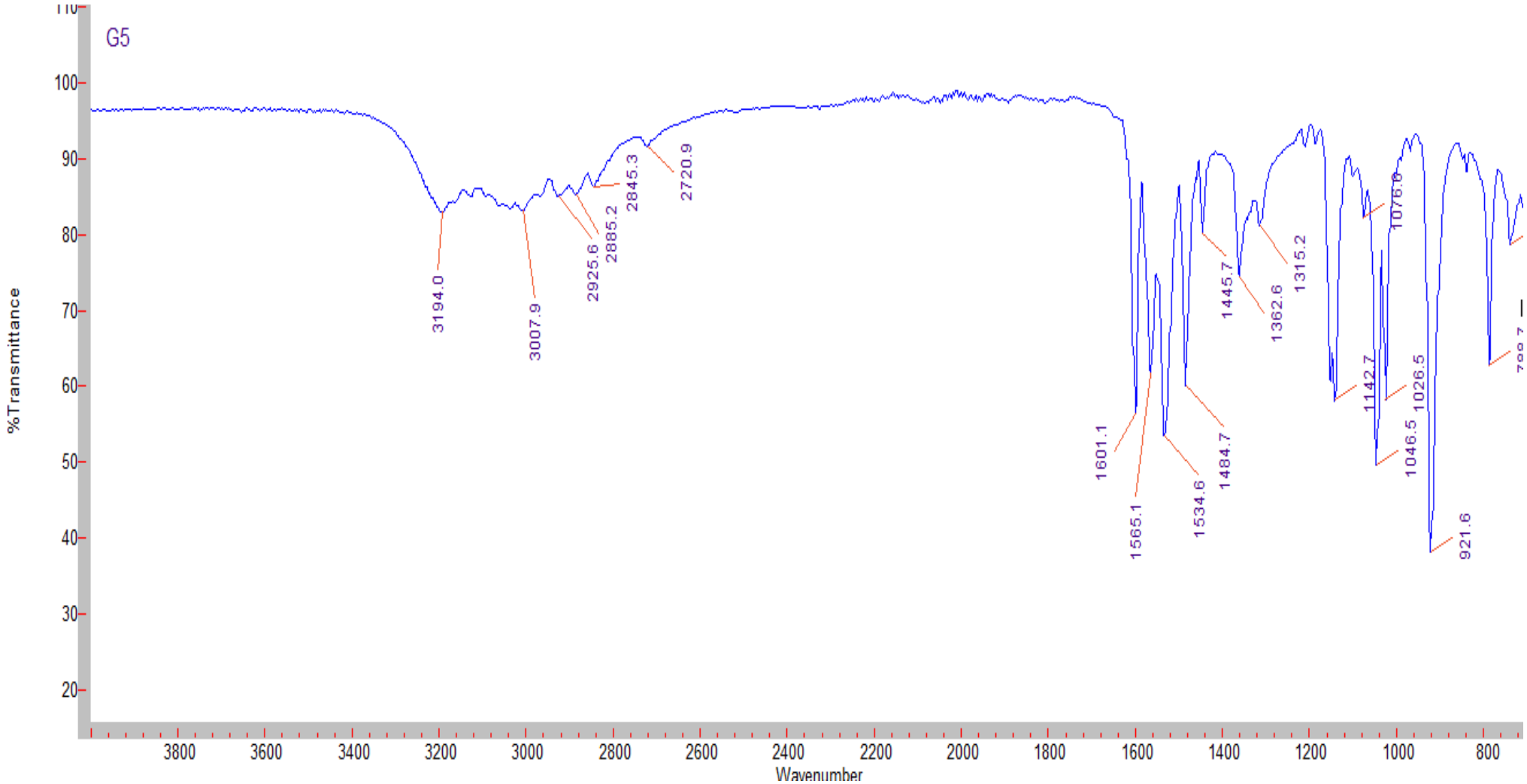
G5
%Transmittance
Wavenumber
3194.0
3007.9
2925.6
2885.2
2845.3
2720.9
1601.1
1565.1
1534.6
1484.7
1445.7
1362.6
1315.2
1142.7
1076.9
1046.5
1026.5
921.6

**6,** [Fe(BPHA)$_3$]

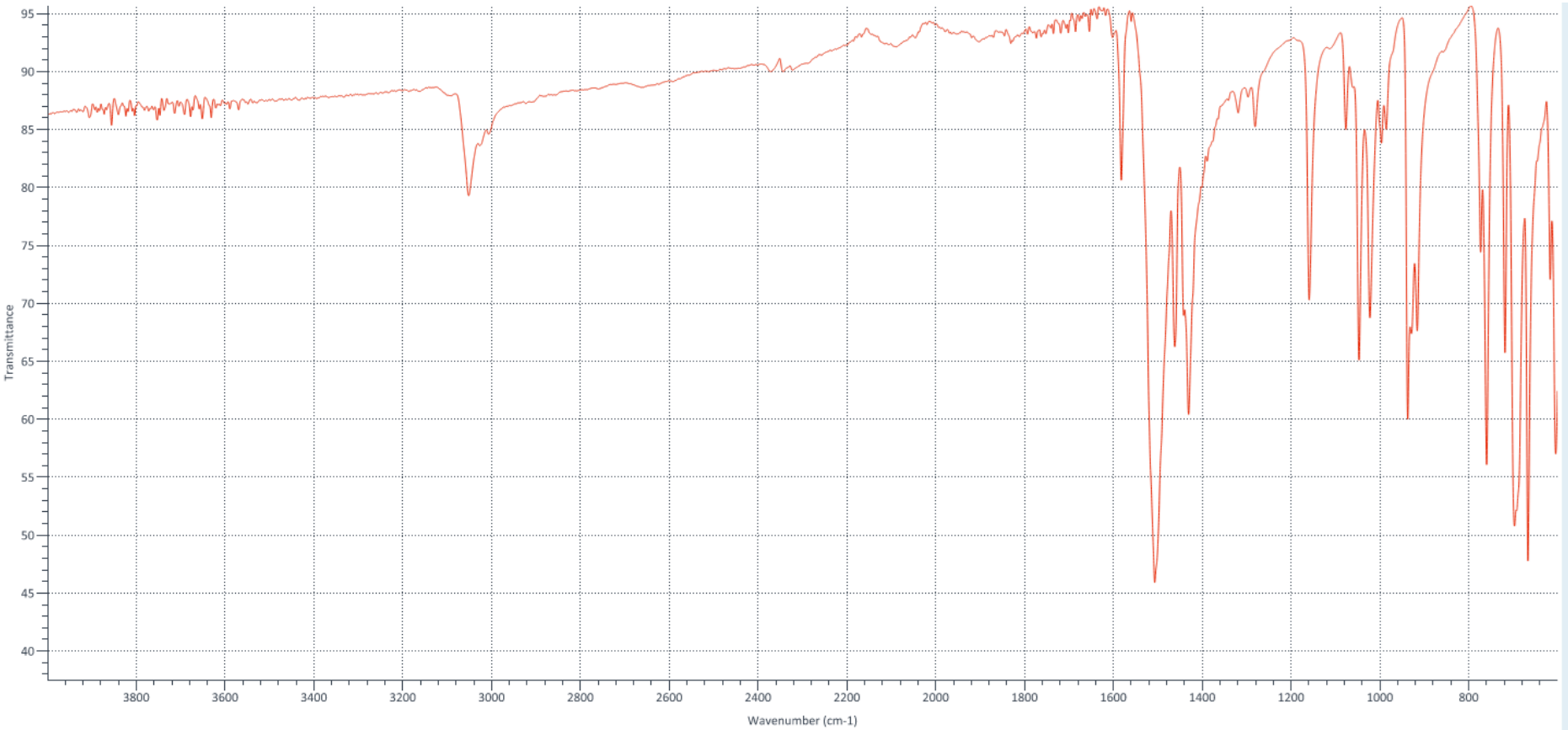
Transmittance
95
90
85
80
75
70
65
60
55
50
45
40
3800
3600
3400
3200
3000
2800
2600
2400
2200
2000
1800
1600
1400
1200
1000
800
Wavenumber (cm-1)

## 3. High-Res Mass Spectrometry of Metal complexes 1 - 6

**1**, $[Ga(BPHA)_3]$

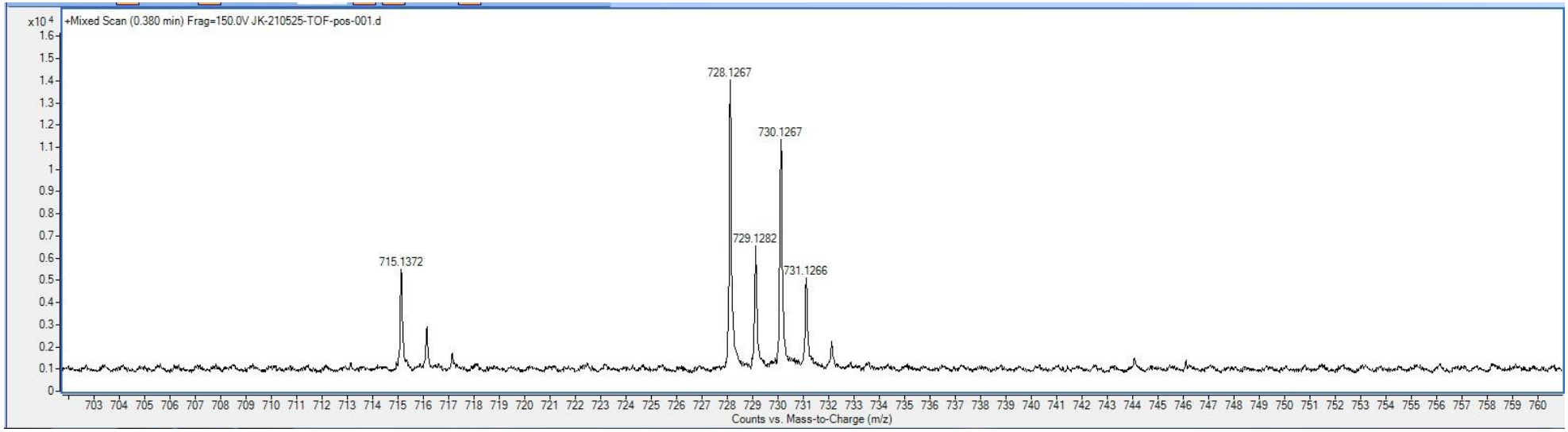


**2,** $[Ga(BHA)_3]$

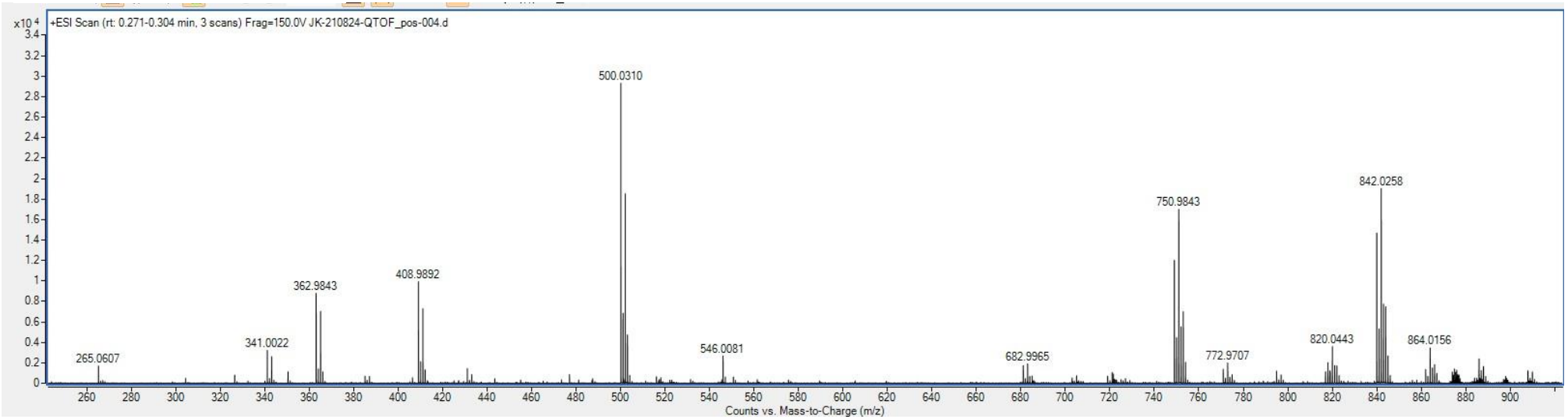

**3**, [Ga(SHA-$H_2$)(SHA-$H$)]

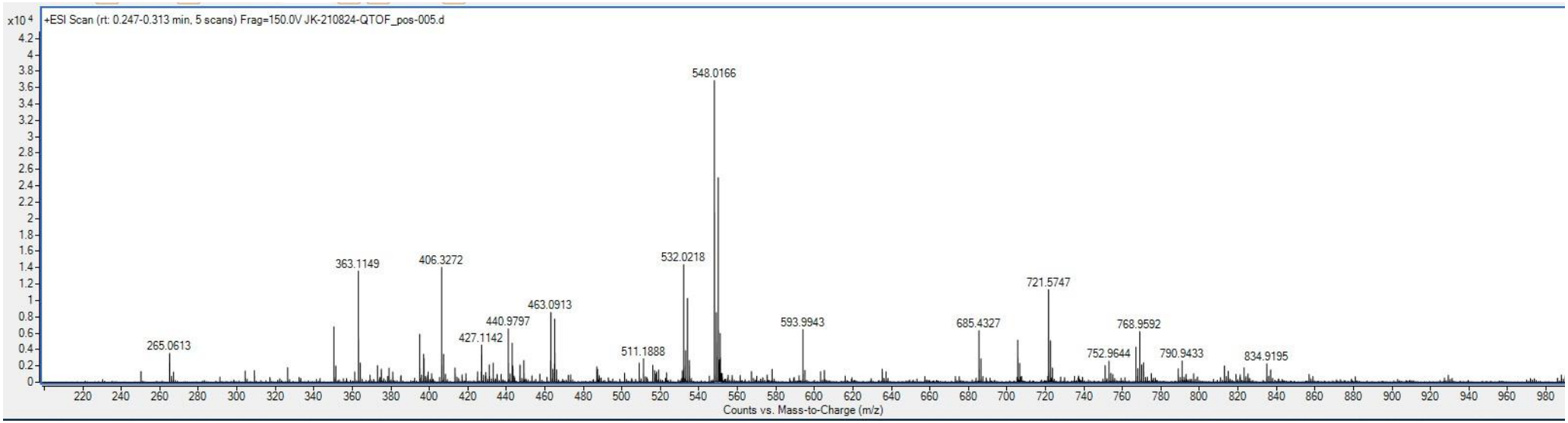


**4,** [$GaMe_2$(BPHA)]

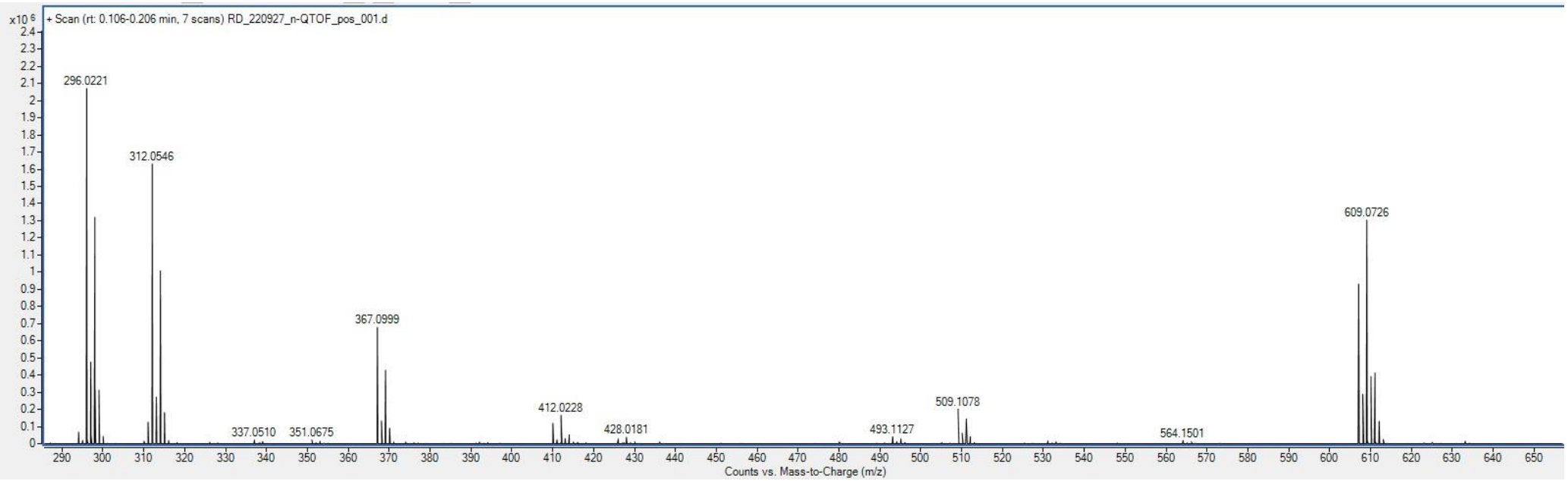

**5**, [GaMe(BHA)$_2$]

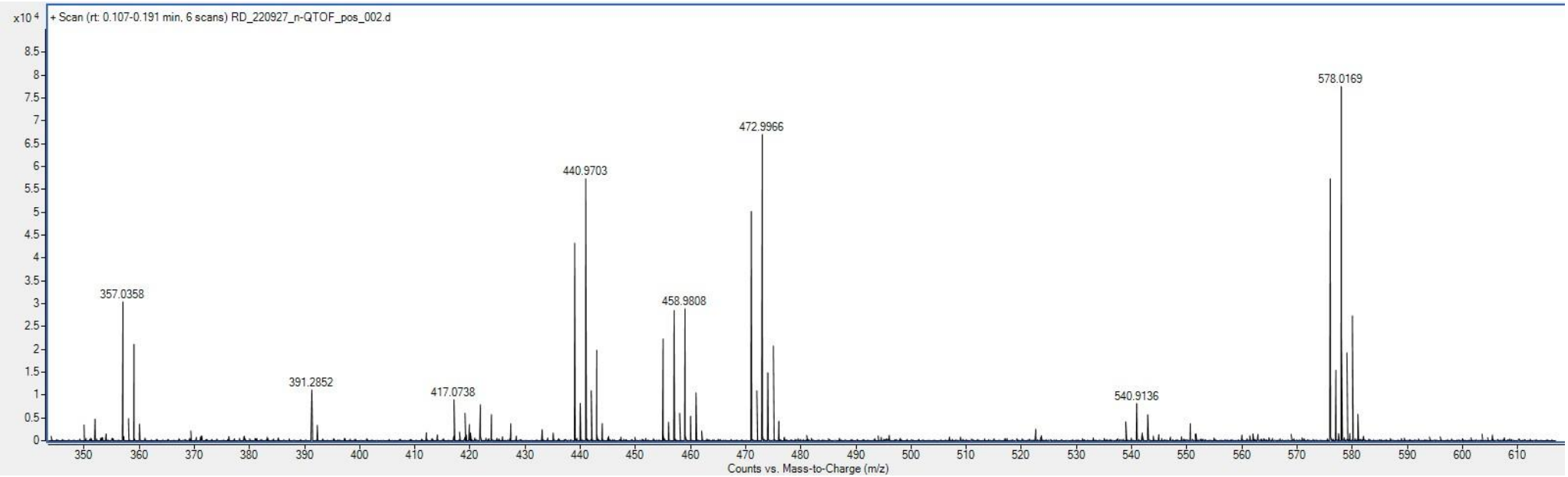


**6,** [Fe(BPHA)$_3$]

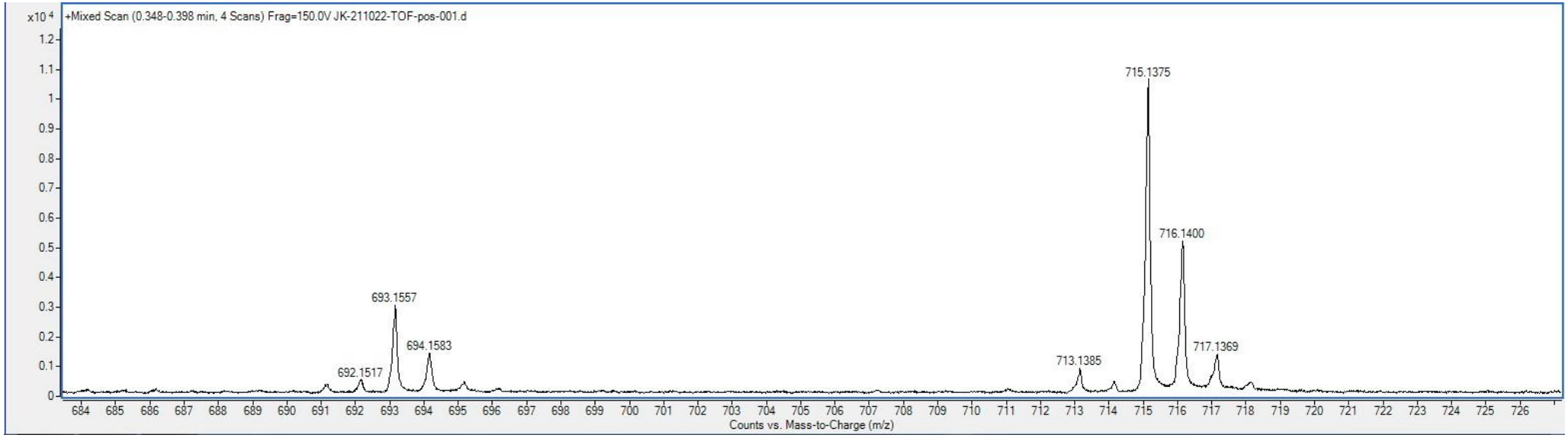

## 4. Additional analytical data

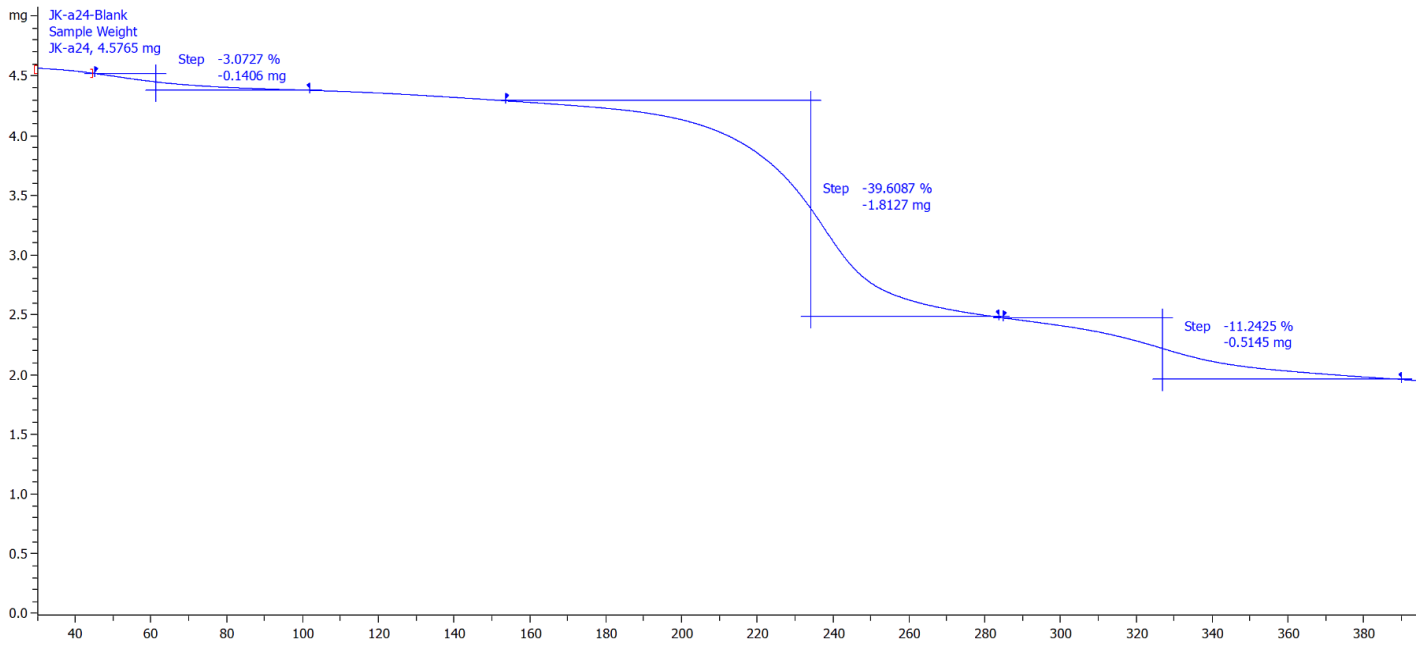


Figure S2. TGA of [Ga(SHAH$_2$)(SHAH)] (**3**), determining the presence of water in the compound.

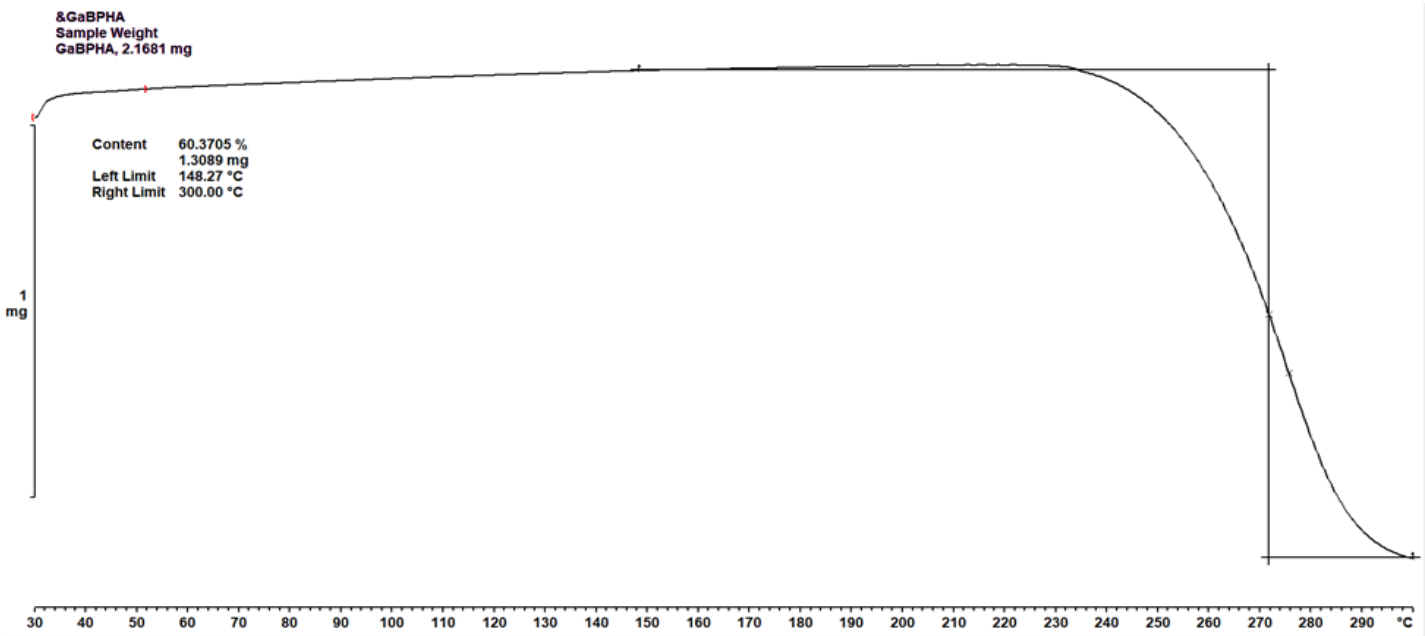


Figure S3. TGA of [Ga(BPHA)$_3$] (1)

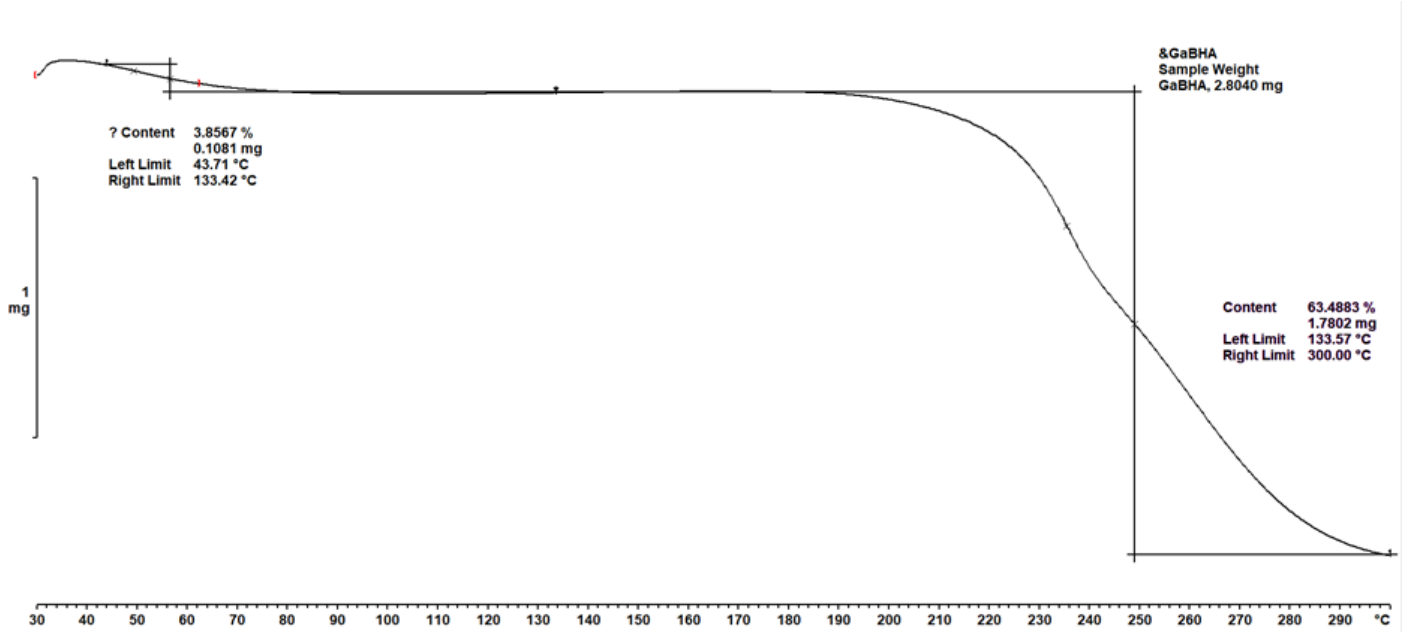


Figure S4. TGA of [Ga(BHA)(BHAH)] (2), determining the presence of water in the compound.

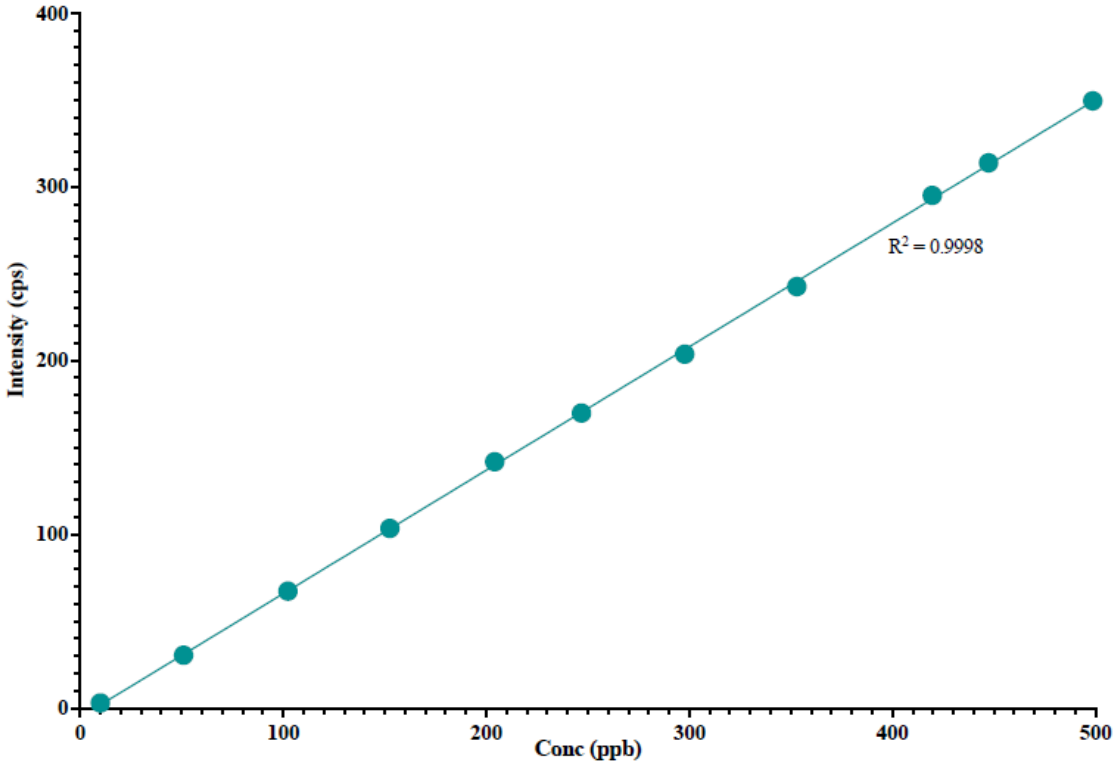


Figure S5. 11-point Gallium-69 calibration curve measured using ICP-MS with an Ag/As internal standard.

## 5. Biological testing

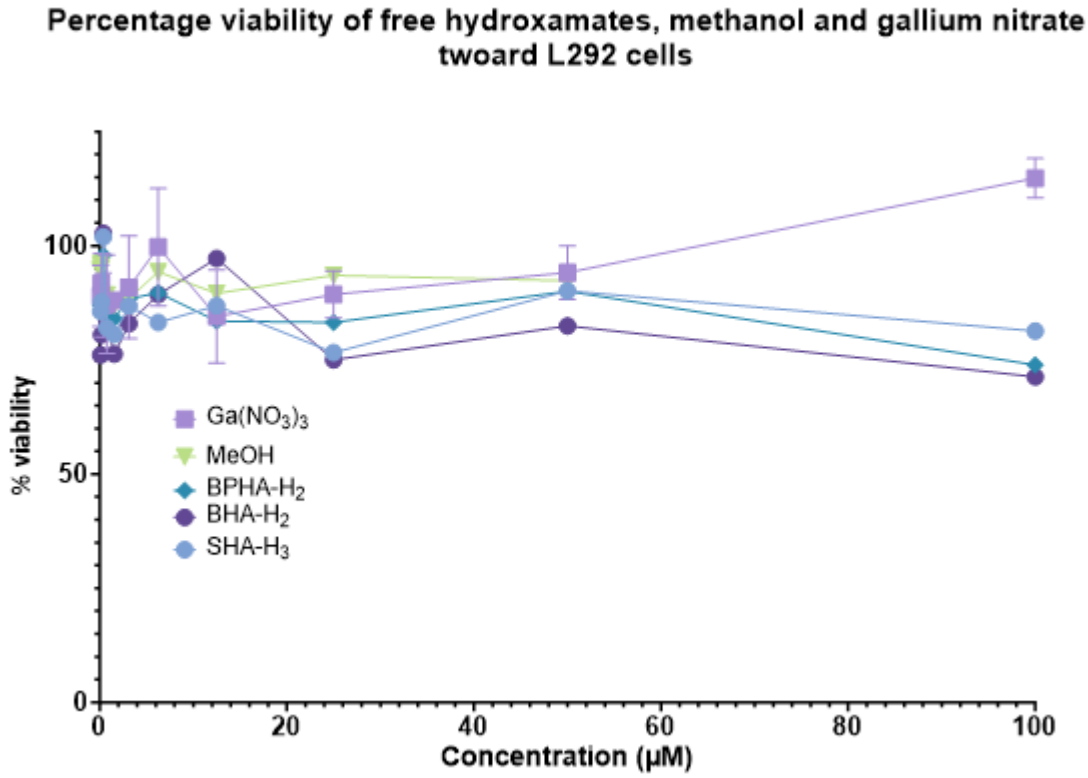


Figure S6. Percentage viability of L929 cells toward controls including free hydroxamic acids: BPHA-$H_2$, BHA-$H_2$, SHA-$H_3$ and gallium nitrate and methanol.

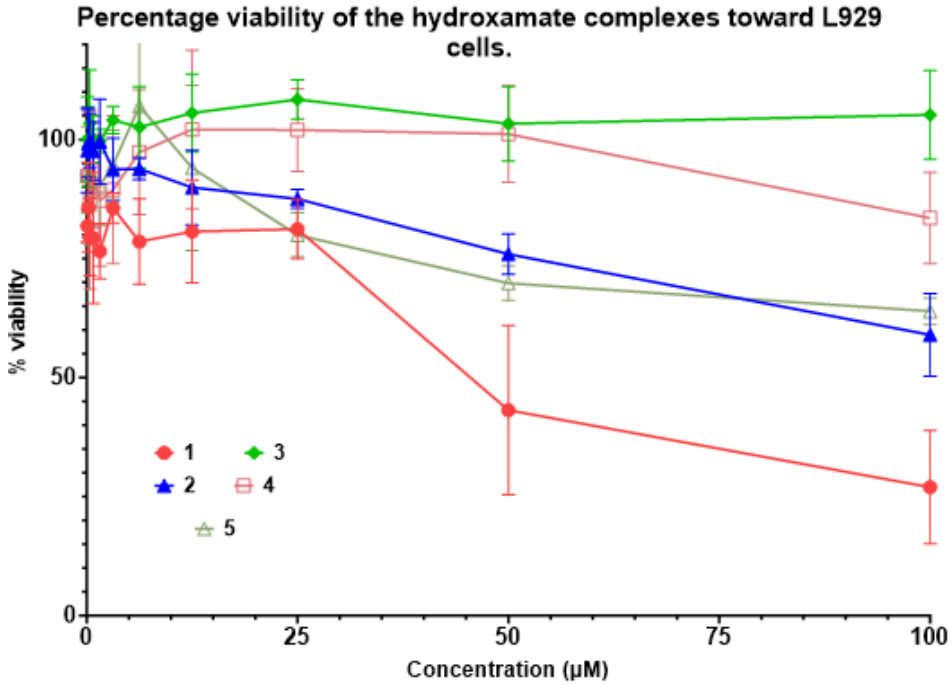


Figure S7. Percentage viability of L929 cells toward gallium complexes [Ga(BPHA)$_3$] **1,** [Ga(BHA-*H*)$_3$] **2**, [Ga(SHA-*H*$_2$)(SHA-*H*)] **3**, [GaMe$_2$(BPHA)] **4,** and [GaMe(BHA-*H*)$_2$] **5**.

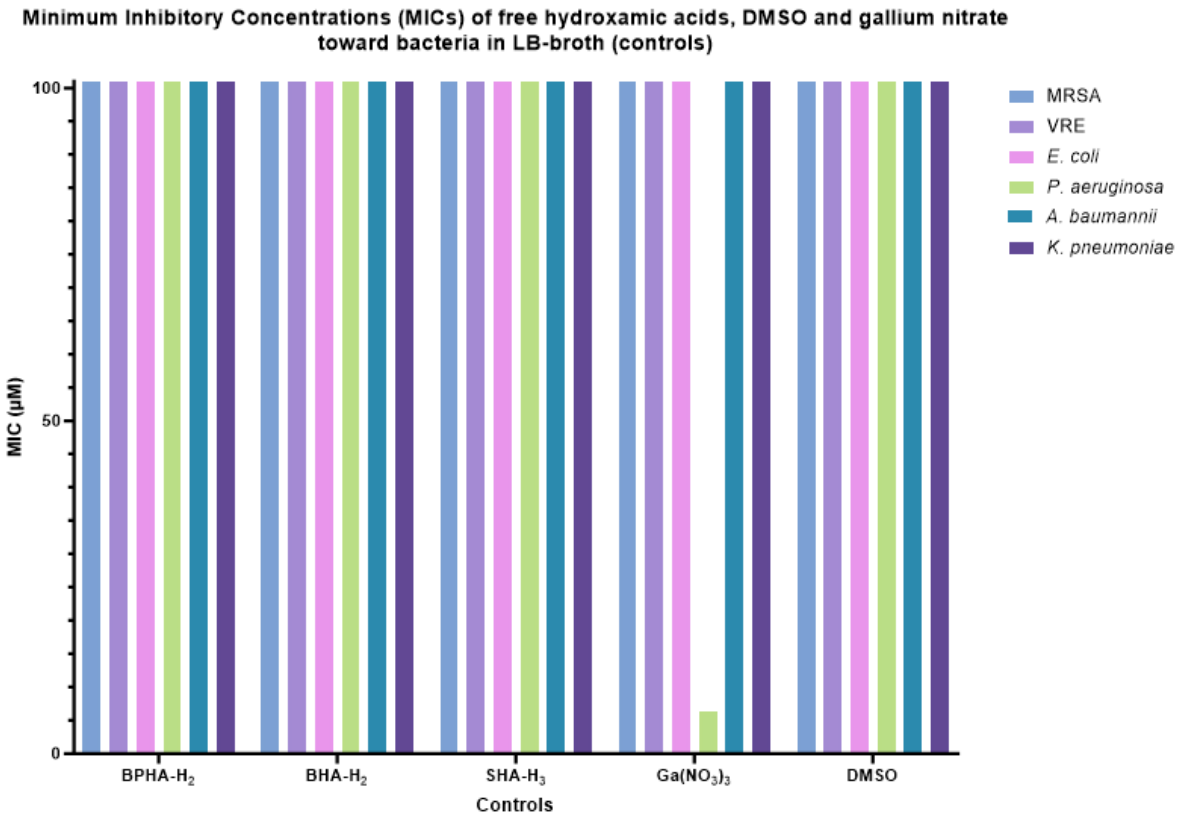


Figure S8. MIC graphs of the controls. including free hydroxamic acids: BPHA-$H_2$, BHA-$H_2$, SHA-$H_3$ and gallium nitrate and DMSO

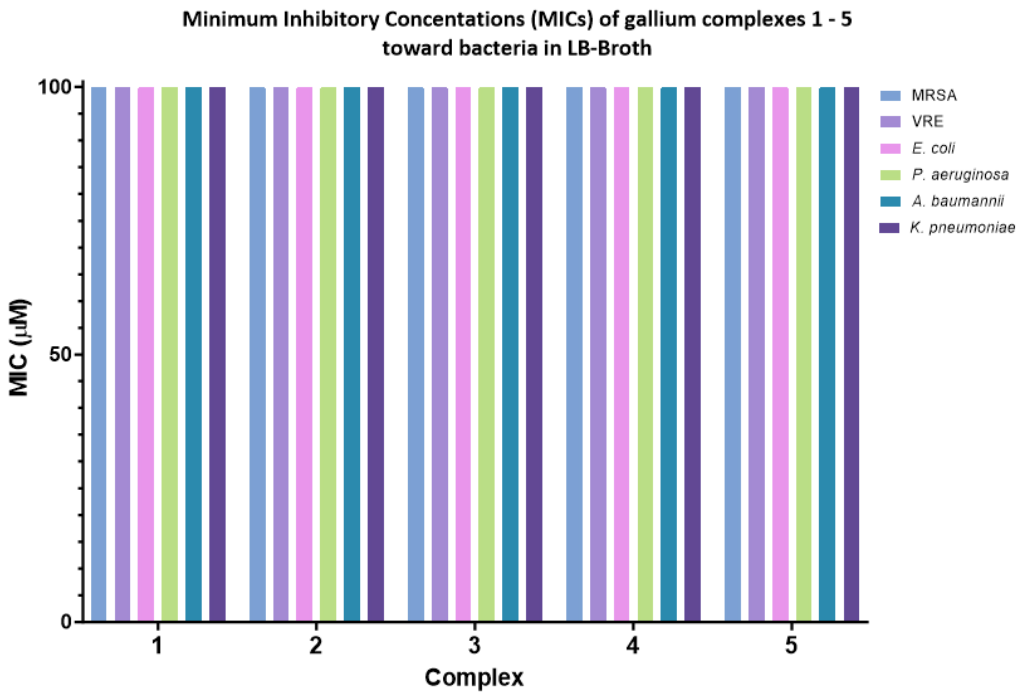


Figure S9. MIC graphs for the gallium complexes [Ga(BPHA)$_3$] **1,** [Ga(BHA-*H*)$_3$] **2**, [Ga(SHA-*H*$_2$)(SHA-*H*)] **3**, [GaMe$_2$(BPHA)] **4,** and [GaMe(BHA-*H*)$_2$] **5** in LB-broth

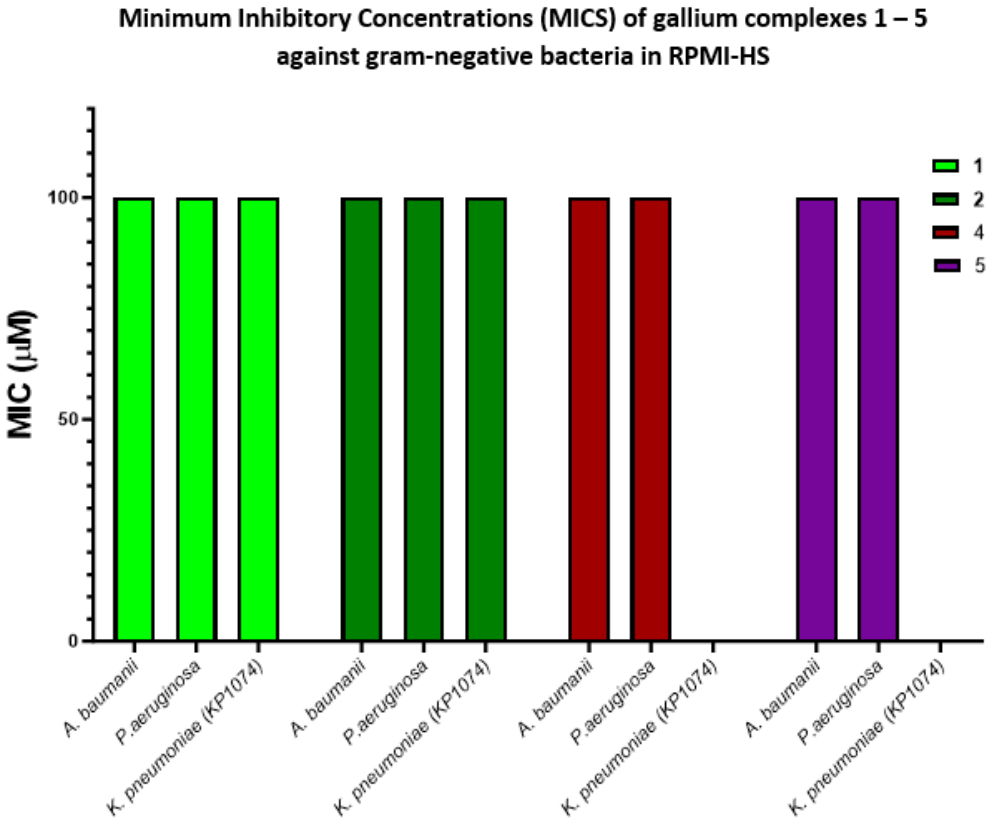


Figure S10. MIC graphs for the gallium complexes Ga(BPHA)$_3$] **1,** [Ga(BHA-*H*)$_3$] **2**, [GaMe$_2$(BPHA)] **4,** and [GaMe(BHA-*H*)$_2$] **5** analysed in RPMI-HS against gram negative bacteria.

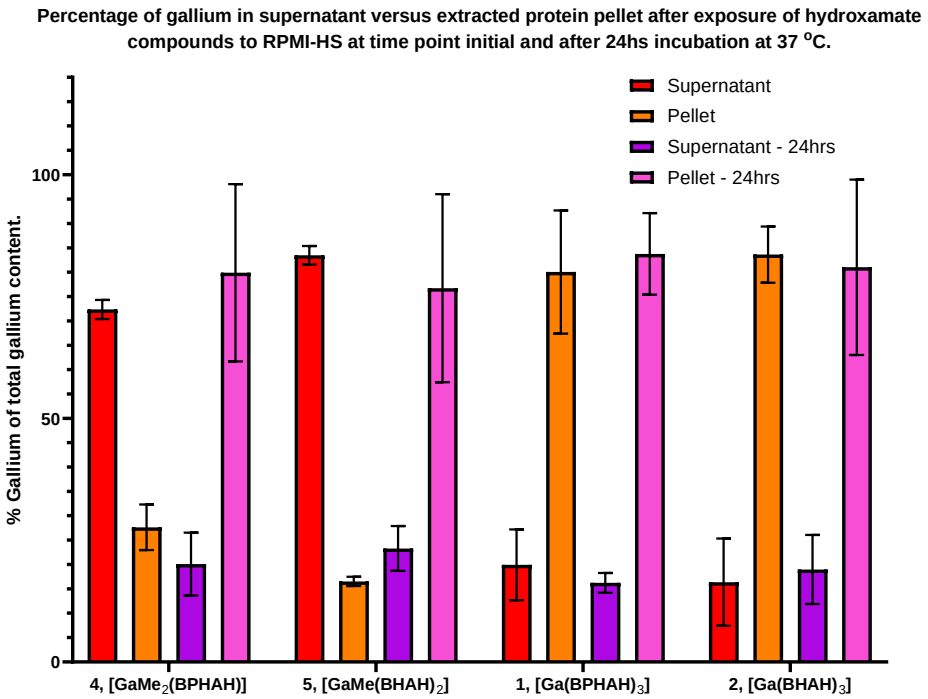


Figure S11. Percentage of gallium observed in the supernatant versus pellet phase of complexes **1**, **2**, **4** and **5**, as a percentage of total gallium in the combined samples. Measurements in triplicate via ICP-MS

## 6. Experimental Section for Complexes 7, 8, 9 and 10

[Ga(BPHA)$_2$(OMe)] **7**:

A few milligrams of solid [Ga(BPHA)$_3$] **1** was sonicated in *ca.* 50 mL of methanol before filtration. A few colourless hexagonal crystals were obtained following slow evaporation of the solvent. Single crystal X-ray diffraction identified them as the methanolysis product [Ga(BPHA)$_2$(OMe)] **7** (Figure S12). CCDC: 2150393

[Ga$_4$(Me)$_7$(BPHA)O$_4$] **8** and [GaMe(BPHA)$_2$] **9:**

Complex **4** [GaMe$_2$(BPHA)] was heated under atmospheric conditions in toluene leading to a small degree of ligand redistribution and partial hydrolysis. Some crystals of the cluster compound [Ga$_4$(Me)$_7$(BPHA)O$_4$] **8** (Figure S13) and the mono-methyl gallium complex [GaMe(BPHA)$_2$] **9** (Figure S14) were identified via single crystal XRD. CCDC **8**: 2330100. CCDC **9**: 2330099.

[{GaMe$_2$(BHA-*H*)}{Ga$_2$Me$_4$O}], **10.**

During the attempted formation of the dimethylgallium complex of benzohydroxamic acid, [{GaMe$_2$(BHA-*H*)] isolated crystals of the polynuclear gallium complex [{GaMe$_2$(BHA-*H*)}{Ga$_2$Me$_4$O}], **10** (Figure S15) were identified by single crystal XRD. CCDC: 2330101.

## 7. X-ray crystallography

Table S1. Detailed bond lengths and angles of 1 and 6

| 1 | | 6 | |
|---|---|---|---|
| **Bond Lengths (Å)** | | | |
| Ga1-O1 | 1.972(18) | Fe1-O1 | 2.002(2) |
| Ga1-O2 | 1.972(18) | Fe1-O1A | 2.002(2) |
| **Bond Angles (˚)** | | | |
| O1-Ga1-O2 | 81.38(10) | O1-Fe1-O1A | 78.59(12) |
| O1-Ga1-O1A | 91.61(8) | O1-Fe1-O1B | 92.41(9) |
| O2-Ga1-O2A | 96.28(12) | O1A-Fe1-O1B | 98.17(14) |

**Crystallographic data:**

Crystallographic data of **1**. $C_{39}H_{30}N_3O_6Ga$, $M_w$ = 706.38, trigonal, space group $P\bar{3}c1$, a = 13.3905(2), b = 13.3905(2), c = 10.3009(3) Å, α = 90, β = 90, γ = 120 ˚, V = 1599.56(7) Å$^3$, Z = 2, density = 1.467 g/cm$^3$, $F_{000}$ = 728, μ = 1.633 mm$^{-1}$, $2\theta_{max}$ = 155.8 ˚, 22506 reflections collected, 1141 unique ($R_{int}$ = 0.0651). Final GooF = 1.067, $R_1$ = 0.0532, $wR_2$ = 0.1493.

Crystallographic data of **4**. $C_{22}H_{23}GaN_2O_4$ (*M* =449.14 g/mol): tetragonal, space group $I4_1/a$ (no. 88), *a* = 22.5883(9) Å, *c* = 16.7968(10) Å, *V* = 8570.3(9) Å$^3$, *Z* = 16, *T* = 123 K, μ(MoKα) = 1.314 mm$^{-1}$, *Dcalc* = 1.392 g/cm$^3$, 23400 reflections measured (4.706° ≤ 2Θ ≤ 52.91°), 4040 unique ($R_{int}$ = 0.0807, $R_{sigma}$ = 0.1117) which were used in all calculations. The final $R_1$ was 0.0295 (I > 2σ(I)) and $wR_2$ was 0.0406 (all data).

Crystallographic data of **5**. $C_{15}H_{16}GaNO_2$ (*M* =312.01 g/mol): monoclinic, space group $P2_1/n$ (no. 14), *a* = 9.7967(3) Å, *b* = 13.9100(3) Å, *c* = 10.3884(3) Å, *β* = 93.174(2)°, *V* = 1413.48(7) Å$^3$, *Z* = 4, *T* = 123.00(10) K, μ(Mo Kα) = 1.943 mm$^{-1}$, *Dcalc* = 1.466 g/cm$^3$, 19008 reflections measured (6.288° ≤ 2Θ ≤ 62.008°), 4017 unique ($R_{int}$ = 0.0404, $R_{sigma}$ = 0.0363) which were used in all calculations. The final $R_1$ was 0.0303 (I > 2σ(I)) and $wR_2$ was 0.0741 (all data).

Crystallographic data of **6.** $C_{39}H_{30}N_3O_6Fe$, $M_w$ = 692.51, trigonal, space group P-3c1 (no. 165), *a* = 13.4603(9) Å, *c* = 10.2309(8) Å, *V* = 1605.3(2) Å$^3$, *Z* = 12, *T* = 123.00(10) K, μ(MoKα) = 0.525 mm$^{-1}$, *Dcalc* = 1.433 g/cm$^3$, 14649 reflections measured (6.992° ≤ 2Θ ≤ 64.472°), 1712 unique ($R_{int}$ = 0.1003,

$R_{sigma}$ = 0.0672) which were used in all calculations. The final $R_1$ was 0.0851 (I > 2σ(I)) and $wR_2$ was 0.2700 (all data).

Crystallographic data of **7**: $C_{27}H_{23}GaN_2O_5$ (*M* =525.19 g/mol): monoclinic, space group $P2_1/c$ (no. 14), *a* = 10.5325(5) Å, *b* = 20.4336(8) Å, *c* = 11.6318(6) Å, *β* = 93.511(5)°, *V* = 2498.7(2) $Å^3$, *Z* = 4, *T* = 123.01(10) K, μ(MoKα) = 1.141 $mm^{-1}$, *Dcalc* = 1.396 $g/cm^3$, 21381 reflections measured (6.702° ≤ 2Θ ≤ 51.978°), 4875 unique ($R_{int}$ = 0.0902, $R_{sigma}$ = 0.0820) which were used in all calculations. The final $R_1$ was 0.0910 (I > 2σ(I)) and $wR_2$ was 0.1690 (all data).

Crystallographic data of **8**. $C_{40}H_{62}Ga_8N_2O_8$, *Mr* = 1256.67, triclinic, *P*-1 (No. 2), a = 9.76440(10) Å, b = 12.35930(10) Å, c = 22.2325(3) Å, α = 85.4710(10)°, β = 86.0980(10)°, γ = 77.3800(10)°, *V* = 2606.49(5) Å3, *T* = 123.00(10) K, *Z* = 2, *Z'* = 1, λ(Cu Kα) = 0.71073, 54923 reflections measured, 11188 unique (*Rint* = 0.0673) which were used in all calculations. The final *wR2* was 0.1285 (all data) and *R1* was 0.0451 (I > 2(I)).

Crystallographic data of **9**. $C_{27}H_{23}GaN_2O_4$, *Mr* = 509.19, space group $P2_1/c$ (no. 14), a = 14.3324(3) Å, b = 9.3198(2) Å, c 18.1798(4) Å, α = 90 β = 98.6 γ = 90° , *V* = 2400.77(9) Å3, *T* = 123.01(13) K, *Z* = 4, *Z'* = 1, λ(Cu Kα) = 0.71073, 31646 reflections measured, 6818 unique (*Rint* = 0.0565) which were used in all calculations. The final *wR2* was 0.0.891 (all data) and *R1* was 0.0393 (I > 2(I)).

Crystallographic data of **10**. $C_{13}H_{24}Ga_3NO_3$, *Mr* = 451.49, orthorhombic, *Pbca* (No. 61), a = 6.9024(2) Å, b = 14.1349(4) Å, c = 37.0932(11) Å, α = β = γ = 90, *V* = 3618.99(18) Å3, *T* = 122.99(11) K, *Z* = 8, *Z'* = 1, λ(Cu Kα) = 0.71073, 19330 reflections measured, 3852 unique (*Rint* = 0.0576) which were used in all calculations. The final *wR2* was 0.1069 (all data) and *R1* was 0.0429 (I > 2(I)).

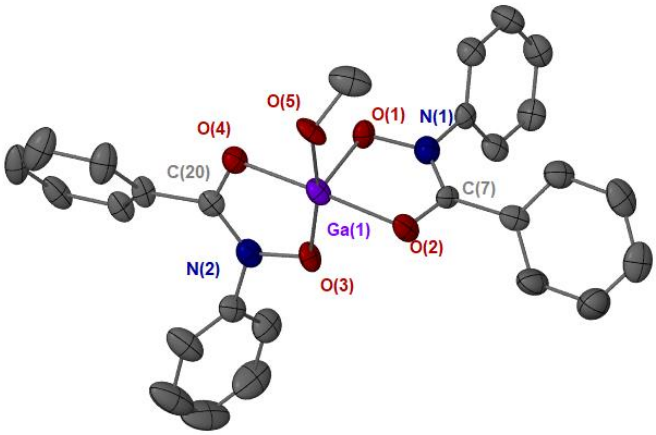


Figure S12. Solid-state structure of [Ga(OMe)(BPHA)$_2$], **7**, as determined by single crystal X-ray diffraction with images generated in Mercury. Thermal ellipsoids at 50 % probability. Hydrogen atoms have been omitted for clarity. Dihydrate in the **7** structure has been omitted for clarity. Selected bond lengths are found in Table 5. Selected bond angles (˚) for **7**: O1-Ga1-O2, 79.62(18), O1-Ga1-O3, 96.53(18), O1-Ga1-O4, 169.5(16), O1-Ga1-O5, 92.32(17), O1-Ga1-O6, 90.29(18).

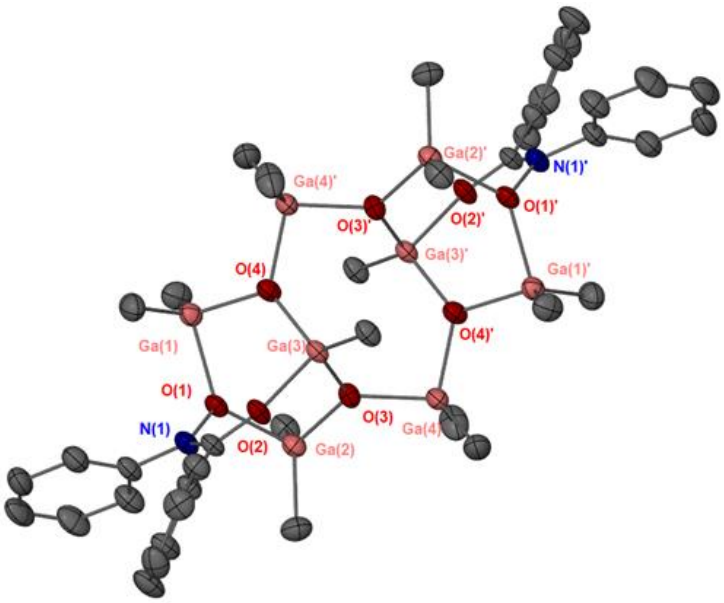


Figure S13. Grown structure of **8**, highlighting the formation of the macrocycle. Thermal ellipsoids at 50%, hydrogen atoms omitted for clarity. Selected bond lengths (Å) and angles (°): Ga(1) – O(1), 2.051(2), Ga(1) – O(4), 1.888(2), Ga(1) – C(14) 1.954(4), Ga(1) – C(15), 1.961(4), Ga(2) – O(1), 2.047(2), Ga(2) – O(3), 1.881(2), Ga(3) – O(2), 1.992(2), Ga(3) – O(3), 1.855(2), Ga(3) – O(4), 1.852(2), Ga(4) – O(3), 1.920(2), Ga(4) – O(4)$'$, 1.914(2). O(4) – Ga(1) – O(1), 92.93(10), O(4) – Ga(1) - C(14), 106.3(2), C(14) – Ga(1) – C(15), 127.9(2), O(3) – Ga(2) – O(2), 94.25(1), Ga(1) – O(1) – Ga(2), 130.5(1), Ga(2) – O(3) – Ga(4), 121.8(1), O(3) – Ga(4) – O(4)$'$, 98.05(1), O(4) – Ga(3) – O(3), 104.5(1). Symmetry operator: **[1]1-X,1-Y,2-Z; [2]1-X,1-Y,1-Z.**

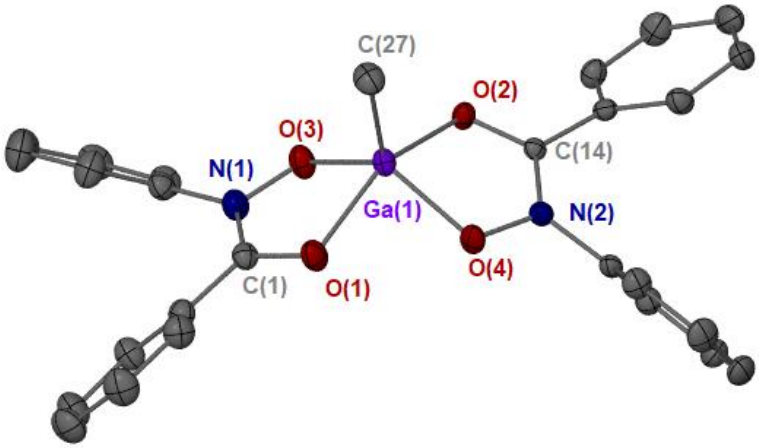


Figure S14. Crystal structure of complex **9,** [GaMe(BPHAH)$_2$], a redistribution product of **4**. Thermal ellipsoids at 50%, hydrogen atoms omitted for clarity. Selected bond lengths (Å) and angles (°): Ga(1) – O(1), 2.024(1), Ga(1) – O(2), 2.202(1), Ga(1) – O(3), 1.932(1), Ga(1) – O(4), 1.932(1), Ga(1) – C(27), 1.958(2). O(1) – Ga(1) – O(2), 150.3(1), O(1) – Ga(1) – O(4) 83.98(6), O(1) – Ga(1) – O(3) 80.91(6), C(27) – Ga(1) – O(1), 114.3(1).

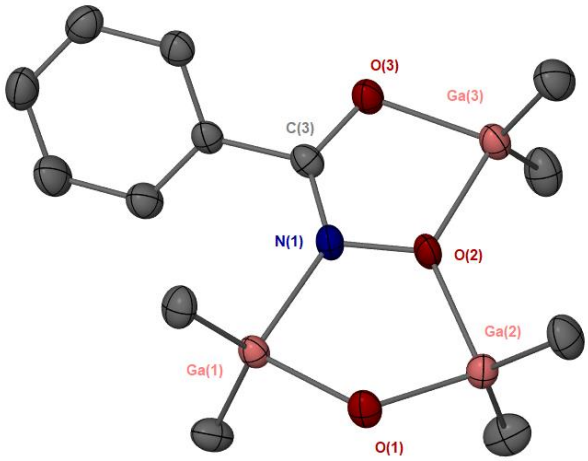


Figure S15. Structure of **10,** [(Ga(Me)$_2$BHAH))(Ga$_2$(Me)$_4$O Thermal ellipsoids at 50%, hydrogen atoms omitted for clarity. Selected bond lengths (Å) and angles (°): Ga(1) – O(1), 1.924(3), Ga(1) – N(1), 2.067(3), Ga(2) – O(1), 1.904(4), Ga(2) – O(2), 1.999(3), Ga(3) – O(2), 1.972(3), Ga(3) – O(3), 1.958(3). Ga(1) – C(1), 1.957(4), Ga(1) – C(2) 1.954(4), Ga(2) – C(1), 1.955(4), Ga(2) – C(11), 1.950(5), Ga(3) – C(12), 1.956(5), Ga(3) – C(13), 1.954(5). O(1) – Ga(1) – N(1), 91.30(12), O(1) – Ga1) – C(1), 104.9(2), C(1) – Ga(1) – C(2), 126.2(2), Ga(2) – O(1) – Ga(1), 119.1(2), O(1) – Ga(2) – O(2), 90.57(12), O(2) – Ga(3) – O(3), 80.80(11), Ga(3) – O(2) – G(2), 127.3(1).

## 8. Biological images

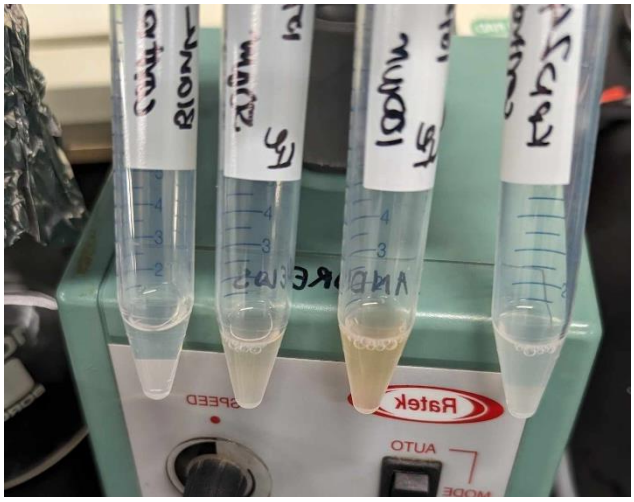

Biological sample of complex **6** at maximum concentration exhibiting no change to opacity when compared to the positive control for *Klebsiella Pneumoniae* KP1074.

Left to right: negative control (clear), **6** 100 µM (opaque), **6** (opaque) 50 µM, positive control (opaque)

Biological sample of complex **1** at minimum inhibitory concentration highlighting the change in opacity to clear when compared to the positive control for *Klebsiella Pneumoniae* KP1074.

Left to right: **4** 0.78 µM (clear), positive control (opaque)

***note label on tubes does not correspond to complex 1***

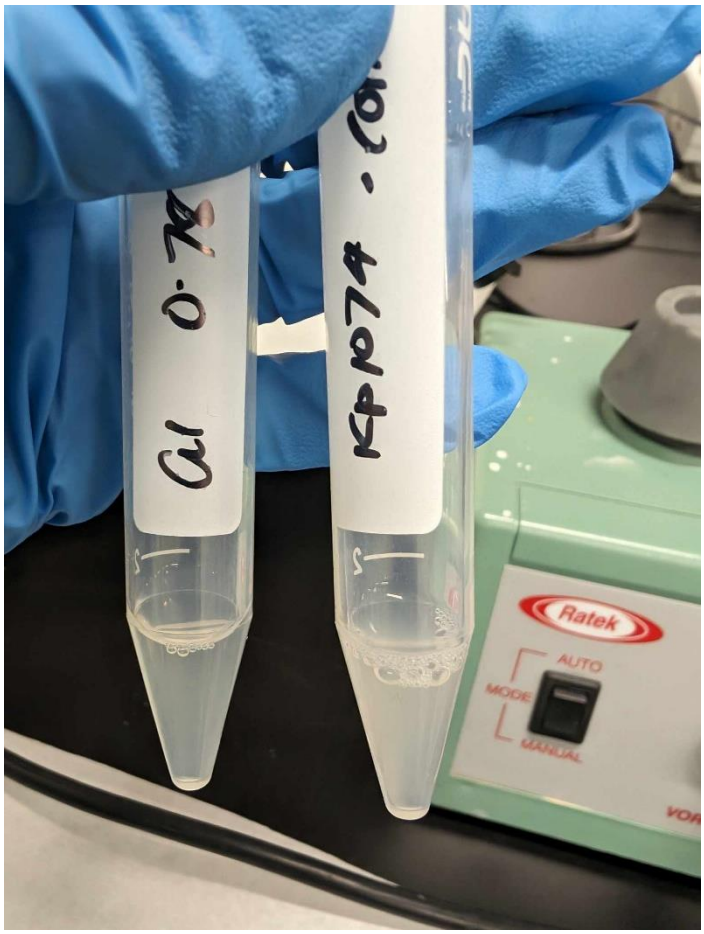

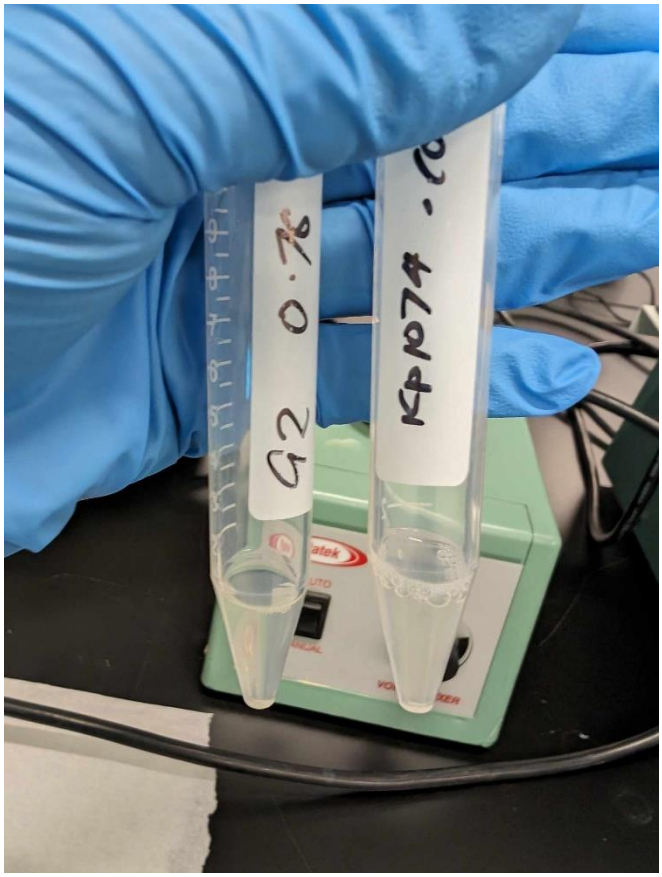


Biological sample of complex **5** at minimum inhibitory concentration highlighting the change in opacity to clear when compared to the positive control for *Klebsiella Pneumoniae* KP1074.

Left to right: **5** 0.78 µM (clear), positive control (opaque)

***note label on tubes does not correspond to complex 2.***

Biological sample of control $GaMe_2OH$ double the concentration of **4** and **5** highlighting no change in opacity when compared to the positive control for *Klebsiella Pneumoniae* KP1074.

Left to right: $GaMe_2OH$ 0.159 µM (clear), positive control (opaque)

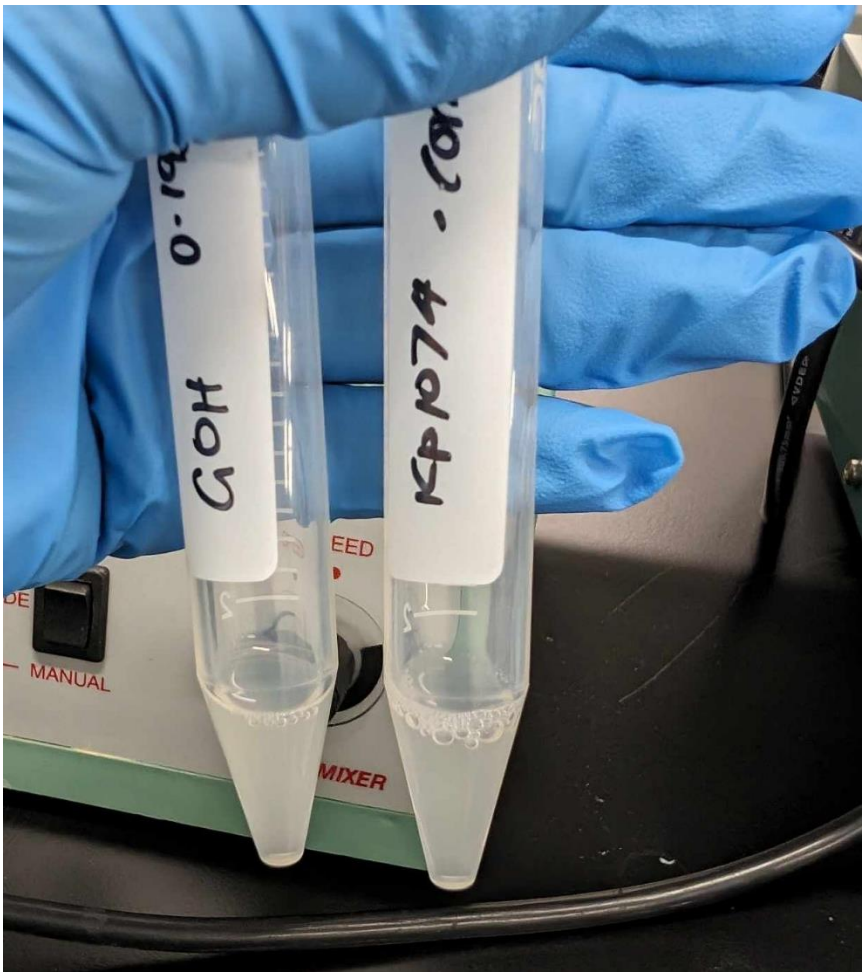

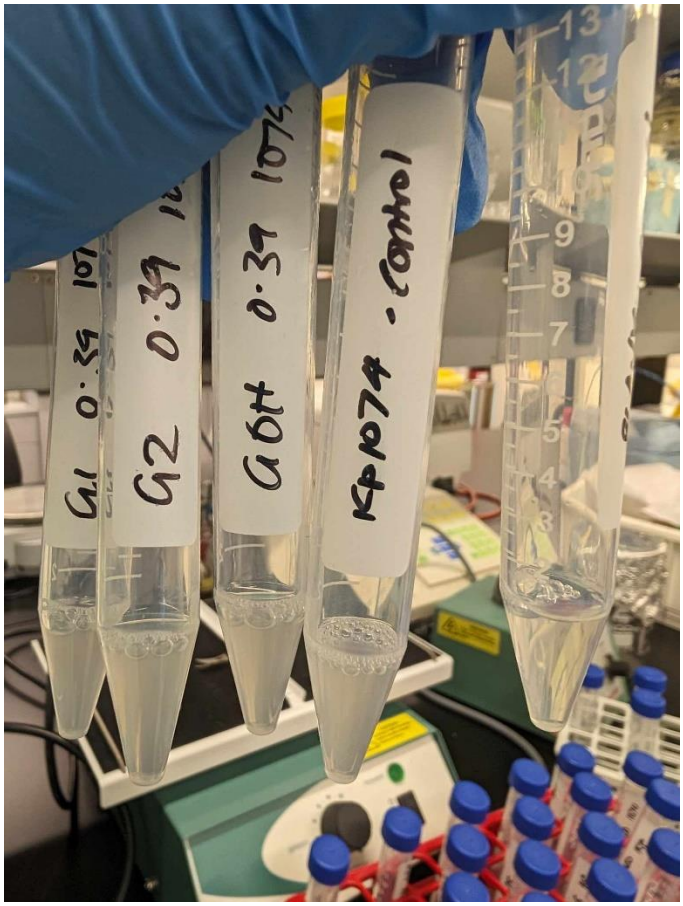


Biological sample of **4**, **5** and control $GaMe_2OH$ at the lowest concentration highlighting no change in opacity when compared to the positive control for *Klebsiella Pneumoniae* KP1074.

Left to right: **4** 0.39 µM (opaque), **5** 0.39 µM (opaque), $GaMe_2OH$ 0.39 µM (opaque), positive control (opaque).

***note label on tubes does not correspond to complexes 1 and 2.***